

An Online Learning Approach to Prompt-based Selection of Generative Models

Xiaoyan Hu*

Ho-fung Leung[†]

Farzan Farnia*

February 11, 2025

Abstract





Selecting a sample generation scheme from multiple text-based generative models is typically addressed by choosing the model that maximizes an averaged evaluation score. However, this score-based selection overlooks the possibility that different models achieve the best generation performance for different types of text prompts. An online identification of the best generation model for various input prompts can reduce the costs associated with querying sub-optimal models. In this work, we explore the possibility of varying rankings of text-based generative models for different text prompts and propose an online learning framework to predict the best data generation model for a given input prompt. The proposed PAK-UCB algorithm addresses a contextual bandit (CB) setting with shared context variables across the arms, utilizing the generated data to update kernel-based functions that predict the score of each model available for unseen text prompts. Additionally, we leverage random Fourier features (RFF) to accelerate the online learning process of PAK-UCB and establish a $\tilde{O}(\sqrt{T})$ regret bound for the proposed RFF-based CB algorithm over T iterations. Our numerical experiments on real and simulated text-to-image and image-to-text generative models show that RFF-UCB performs successfully in identifying the best generation model across different sample types.





1 Introduction

Text-based generative artificial intelligence (AI) has found numerous applications in various engineering tasks. A prompt-based generative AI represents a conditional generative model that produces samples given an input text prompt. Over the past few years, several frameworks using diffusion models and generative adversarial networks have been proposed to perform text-guided sample generation tasks for various data domains including image, audio, and video (Reed et al., 2016; Pan et al., 2018; Xu et al., 2018; Ding et al., 2021; Singer et al., 2022; Huang et al., 2023; Podell et al., 2024). The multiplicity of developed prompt-based models has led to significant interest in developing evaluation mechanisms to rank the existing models and find the best generation scheme. To address this task, several evaluation metrics have been proposed to quantify the fidelity and relevance of samples created by prompt-based generative models, such as CLIPScore (Hessel et al., 2021) and PickScore (Kirstain et al., 2023).

*Department of Computer Science and Engineering, The Chinese University of Hong Kong. Email Address: {xyhu21,farnia}@cse.cuhk.edu.hk

[†]Independent Researcher. Email Address: ho-fung.leung@outlook.com

Example 1	Stable Diffusion v1.5	PixArt- α
Prompts of Type “dog”		
avg. CLIPScore	36.37 (± 0.13)	37.24 (± 0.09)
Prompts of Type “car”		
avg. CLIPScore	36.10 (± 0.06)	35.68 (± 0.15)

Example 2	UniDiffuser	Stable Diffusion v1.5
Prompts of Type “elephant”		
avg. CLIPScore	36.67 (± 0.05)	35.08 (± 0.06)
Prompts of Type “fire hydrant”		
avg. CLIPScore	35.11 (± 0.14)	37.23 (± 0.05)

(a): Example 1: Stable Diffusion v1.5 attains a higher CLIPScore in generating prompts with term “car” (36.10 versus 35.68) while underperforms for prompts with term “dog” (36.37 versus 37.24).

(b): Example 2: UniDiffuser attains a higher CLIPScore in generating prompts with the term “elephant” (36.67 versus 35.08) while underperforms for prompts with the term “fire hydrant” (35.11 versus 37.23).

Figure 1: Standard text-to-image (T2I) models exhibit different rankings based on CLIPScore (Hessel et al., 2021) across the text prompts.

The existing model selection methodologies commonly aim to identify the generative model with the highest relevance score, producing samples that correlate the most with input text prompts. A well-known example is the CLIPScore for image generation models, measuring the expected alignment between the input text and output image of the model using the CLIP embedding (Radford et al., 2021a). While the best-model identification strategy has been frequently utilized in generative AI applications, this approach does not consider the possibility that the involved models can perform differently across text prompts. However, it is possible that one model outperforms another model in responding to text prompts from certain categories, while that model performs worse in generating samples for other text categories. Figure 1 shows such examples where two standard text-to-image models exhibit different rankings across the text prompts with terms “dog”/“car” and “elephant”/“fire hydrant”. In general, the different training sets and model architectures utilized to train text-based models can result in the models’ varying performance in response to different text prompts, which is an important consideration in the selection of text-based generative models for various text prompts.

In this work, we aim to develop a learning algorithm to identify the best generative model for a given input prompt, using observed prompt/generated samples collected from the models in the previous sample generation iterations. Since the goal of such text-based model selection is to minimize the data queries from suboptimal generative models for an input text prompt, we view the model selection task as an online learning problem, where after each data generation the learner updates the prediction on which generative model performs the best in response to

different text prompts. Here, the goal of the online learner is to utilize the previously generated samples to accurately guess the generation model with the best performance for the incoming text prompt. An optimal online model selection method will result in a bounded regret value, measured in comparison to the sample generation from the groundtruth-best model for the text prompts.

The described online learning task can be viewed as a *contextual bandit (CB)* problem studied in the bandit literature (Langford and Zhang, 2007; Li et al., 2010). In the CB task, the online learner observes a single context variable (the text prompt in our setting) and predicts the best arm for the current input context. Specifically, we focus on the kernel-based method to predict the score of each available model for an incoming prompt. As the text prompt is shared across the models, the CB task may be suboptimally addressed by the standard linear CB (Chu et al., 2011) and kernelized CB (Valko et al., 2013) algorithms in the literature, as these algorithms train a single model to predict the reward functions for all the arms. To relax this constraint, we propose Per-Arm Kernelized UCB (PAK-UCB) to address the online prompt-based selection of generative models. According to the PAK-UCB approach, the learner utilizes UCB-scores from arm-specific kernel-based prediction functions to choose the generative model for the incoming text prompt and subsequently update the kernel-based prediction rule based on the generated data for the upcoming iterations. We prove that the proposed PAK-UCB achieves an $\tilde{O}(\sqrt{T})$ regret bound over a horizon of T iterations.

Since the user applying the CB-based model selection approach may have limited compute power and not be able to afford growing computational costs in the online learning process, we propose to utilize the random Fourier features (RFF) framework (Rahimi and Recht, 2007a) to balance the computational load between the iterations of PAK-UCB. We discuss that in the proposed PAK-UCB, the computational cost per iteration will grow cubically as $O(t^3)$ with iteration t . To address the growing cost per iteration of kernel-UCB, we leverage the RFF approach and develop the proxy RFF-UCB algorithm which approximates the solution to PAK-UCB, while the computational costs grow only linearly $O(t)$. We show that the regret bound for PAK-UCB will approximately hold for RFF-UCB, and therefore, RFF-UCB provides an efficient proxy to the PAK-UCB algorithm, which can be run in devices with lower computation budget.

Finally, we present the results of several numerical experiments to show the efficacy of our proposed PAK-UCB and RFF-UCB in the online selection of conditional generative models. In our experiments, we test several pre-trained and simulated text-to-image and image-captioning (image-to-text) models, where different models lead to different rankings of CLIPScore values across sample types. Our numerical results suggest a fast convergence of the proposed online learning algorithms to the best model available for different prompt types. Moreover, we apply the RFF-UCB method and show how the algorithm can infer the model with higher CLIPScore with a growing accuracy as the iteration grows. In our experiments, the proposed PAK-UCB and RFF-UCB outperform various baseline methods including the standard LinUCB (Chu et al., 2011) and KernelUCB (Valko et al., 2013) methods. The main contributions of our work can be summarized as:

- Studying the prompt-based selection of conditional generative models to improve the performance scores over every individual model
- Developing the contextual bandit-based PAK-UCB and RFF-UCB algorithms for the online selection of prompt-based generative models
- Providing the theoretical analysis of the regret and computational costs of PAK-UCB and RFF-

UCB online learning methods

- Presenting numerical results on the online selection of generative models based on the incoming prompt using PAK-UCB and RFF-UCB

2 Related Work

(Automatic) Evaluation of conditional generative models. Evaluating the conditional generative models has been studied extensively in the literature. For text-to-image (T2I) generation, earlier methods primarily rely on the Inception score (Salimans et al., 2016) and Fréchet inception distance (Heusel et al., 2017). More recent works propose reference-free metrics for robust automatic evaluation of T2I and image captioning, with notable examples being CLIPScore (Hessel et al., 2021) and PickScore (Kirstain et al., 2023). Kim et al. (2022) propose a mutual-information-based metric, which attains consistency across benchmarks, sample parsimony, and robustness. To provide a holistic evaluation of T2I models, several works focus on multi-objective evaluation. Astolfi et al. (2024) propose to evaluate conditional image generation in terms of *prompt-sample consistency*, *sample diversity*, and *fidelity*. Kannen et al. (2024) introduce a framework to evaluate T2I models regarding *cultural awareness* and *cultural diversity*. Masrourisaadat et al. (2024) examine the performance of several T2I models in generating images such as human faces and groups and present a social bias analysis. Another line of study explores evaluation approaches using large language models (LLMs). Tan et al. (2024) develop LLM-based evaluation protocols that focus on the *faithfulness* and *text-image alignment*. Peng et al. (2024) introduce a GPT-based benchmark for evaluating personalized image generation. For evaluation of text-to-video (T2V) generation, Huang et al. (2024) introduce VBench as a comprehensive evaluation of T2V models in terms of *quality* and *consistency*.

(Kernelized) Contextual bandits. The contextual bandits (CB) is an efficient framework for online decision-making with side information (Langford and Zhang, 2007; Foster et al., 2018), which is widely adopted in domains such as recommendation system and online advertisement (Li et al., 2010). A key to its formulation is the relationship between the context (vector) and the expected reward. In linear CB, the reward is assumed to be linear to the context vector (Li et al., 2010; Chu et al., 2011). To incorporate non-linearity, Valko et al. (2013) propose kernelized CB, which assumes the rewards are linear-realizable in a reproducing kernel Hilbert space (RKHS). To address the growing computation, recent work leverages the assumption that the kernel matrix is often approximately low-rank and uses Nyström approximations (Calandriello et al., 2019, 2020; Zenati et al., 2022).

3 Preliminaries

3.1 CLIPScore

CLIPScore (Hessel et al., 2021) is a widely used automatic metric to evaluate the alignment of text-to-image/video (T2I/V) and image captioning models. Let $(y, x) \in \mathcal{Y} \times \mathcal{X}$ be any *text-image pair*. We denote by $\mathbf{c}_y \in \mathbb{S}^{d-1} := \{z \in \mathbb{R}^d : \|z\|_2 = 1\}$ and $\mathbf{v}_x \in \mathbb{S}^{d-1}$ the (normalized) embeddings of text $y \in \mathcal{Y}$ and image $x \in \mathcal{X}$, respectively, both extracted by CLIP (Radford et al., 2021b). The

CLIPScore (Hessel et al., 2021) is given by

$$\text{CLIPScore}^{\text{T2I}}(y, x) := \max\{0, 100 \cdot \cos(\mathbf{v}_x, \mathbf{c}_y)\}, \quad (1)$$

and note that $\cos(\mathbf{v}_x, \mathbf{c}_y) = \langle \mathbf{v}_x, \mathbf{c}_y \rangle$ as we operate under the normalized embeddings. Further, for a video $X := \{x^{(l)}\}_{l=1}^L$ consisting of L frames, where $x^{(l)}$ is the l -th frame, the score is the averaged frame CLIPScore, that is,

$$\text{CLIPScore}^{\text{T2V}}(y, X) := \frac{1}{L} \sum_{l=1}^L \text{CLIPScore}^{\text{T2I}}(y, x^{(l)}). \quad (2)$$

3.2 Kernel Methods and Random Fourier Features

Let $\phi : \mathbb{R}^d \rightarrow \mathcal{H}$ denote a mapping from the *primal space* \mathbb{R}^d to the (possibly infinite-dimensional) associated *reproducing kernel Hilbert space* (RKHS) \mathcal{H} . The corresponding *kernel function* is defined by $k(y, y') := (\phi(y))^\top \phi(y')$ for any $y, y' \in \mathbb{R}^d$. The kernel function k is *positive definite* if $\sum_{i=1}^n \sum_{j=1}^n c_i c_j k(y_i, y_j) \geq 0$ for any $n \in \mathbb{N}_+$, $y_1, \dots, y_n \in \mathbb{R}^d$, and $c_1, \dots, c_n \in \mathbb{R}$. Further, a positive definite kernel function is *shift invariant* if $k(y, y') := k(y - y')$ for any $y, y' \in \mathbb{R}^d$. An example is the *radial basis function* (RBF) kernel:

$$k_{\text{RBF}}(y, y') = \exp(-\|y - y'\|_2^2 / (2\sigma^2)),$$

where $\sigma > 0$.

Kernel ridge regression (KRR). Given empirical data $(y_1, s_1), \dots, (y_n, s_n)$, where $\{y_i \in \mathbb{R}^d\}_{i=1}^n$ are *dependent variables* and $\{s_i \in \mathbb{R}\}_{i=1}^n$ are *target variables*, respectively, the kernel method assumes the existence of $w^* \in \mathcal{H}$ such that $\mathbb{E}[s_i | y_i] = (\phi(y_i))^\top w^*$ for any $i = 1, \dots, n$. Let $\alpha \geq 0$ denote a *regularization parameter*. KRR constructs the estimator

$$\hat{s}_{\text{KRR}}(y) := k_y^\top (K + \alpha I_n)^{-1} v$$

for any $y \in \mathbb{R}^d$, where $K = [k(y_i, y_j)]_{i,j=1}^n \in \mathbb{R}^{n \times n}$ is the kernel matrix, $v := [s_1, \dots, s_n]^\top \in \mathbb{R}^n$, and $k_y = [k(y_1, y), \dots, k(y_n, y)]^\top \in \mathbb{R}^n$. The estimator can be interpreted as first estimating w^* by ridge regression

$$\hat{w} := \arg \min_{w \in \mathcal{H}} \sum_{i=1}^n ((\phi(y_i))^\top w - s_i)^2 + \alpha \|w\|,$$

where $\|w\| := \sqrt{w^\top w}$ for any $w \in \mathcal{H}$, and then making the prediction $\hat{s}_{\text{KRR}}(y) = (\phi(y))^\top \hat{w}$.

Random Fourier features (RFF). One problem of KRR is that it scales poorly with the size n of the empirical data, i.e., computing the KRR estimator generally requires $\Omega(n^3)$ time and $\Omega(n^2)$ memory. To address this problem, Rahimi and Recht (2007b) propose to scale up kernel methods by RFF sampling. Specifically, the Bochner’s Theorem (Rudin, 2017) implies that for any (properly scaled) shift-invariant kernel $k(y, y') = k(y - y')$, there exists a distribution $p \in \Delta(\mathbb{R}^d)$ such that $k(y, y') = \mathbb{E}_{w \sim p}[e^{i w^\top (y - y')}]$, where $e^{i\theta} := \cos \theta + i \cdot \sin \theta$ for any $\theta \in \mathbb{R}$ and i is the *imaginary unit*. Therefore, the idea of RFF is to sample $w_1, \dots, w_s \sim p$ and approximate $k(y, y')$ by the empirical

mean $s^{-1} \sum_{j=1}^s e^{iw_j^\top (y-y')}$ to within ϵ with only $s = O(d\epsilon^{-2} \log(1/\epsilon^2))$. Since the kernel $k(\cdot)$ is real, we can replace the complex exponentials with cosines and define

$$\varphi(y) := \sqrt{\frac{2}{s}} \cdot [\cos(w_1^\top y + b_1), \dots, \cos(w_s^\top y + b_s)]^\top, \quad (3)$$

where $\{w_j\}_{j=1}^s \stackrel{\text{i.i.d.}}{\sim} p$, $\{b_j\}_{j=1}^s \stackrel{\text{i.i.d.}}{\sim} \text{Unif}([0, 2\pi])$, and $k(y, y')$ is approximated by $(\varphi(y))^\top \varphi(y')$. The resulting approximate KRR estimator

$$\tilde{s}_{\text{KRR}}(y) := (\tilde{\Phi}^* \tilde{\Phi} + \alpha I_s)^{-1} \tilde{\Phi}^* v,$$

where $\Phi := [\varphi(y_i)]_{i=1}^n \in \mathbb{C}^{n \times s}$, can be computed in $O(ns^2)$ time and $O(ns)$ memory, giving substantial computational savings if $s \ll n$ (Avron et al., 2017). For the RBF kernel, the distribution p_{RBF} is the multivariate Gaussian $\mathcal{N}(0, \sigma^{-2} \cdot I_d)$.

4 Prompt-Based Selection as Contextual Bandits

In this section, we introduce the framework of online prompt-based selection of generative models, which is given in Protocol 1. Let $[N] := \{1, \dots, N\}$ for any positive integer $N \in \mathbb{N}_+$. We denote by $\mathcal{G} := [G]$ the set of (prompt-based) generative models. The evaluation proceeds in $T \in \mathbb{N}_+$ iterations.

At each iteration $t \in [T]$, a *prompt* $y_t \in \mathcal{Y}$ is drawn from a fixed distribution $\rho \in \Delta(\mathcal{Y})$ on the prompt space $\mathcal{Y} \subseteq \mathbb{S}^{d-1}$, e.g., (the normalized embedding of) a picture in image captioning or a paragraph in text-to-image/video generation. Based on prompt y_t (and previous observation sequence), an algorithm \mathcal{A} picks model $g_t \in \mathcal{G}$ and samples an *answer* $x_t \sim P_{g_t}(\cdot | y_t)$, where $P_g(\cdot | y) \in \Delta(\mathcal{X})$ is the conditional distribution of answers generated from any model $g \in \mathcal{G}$. The quality of answer x_t is evaluated using a *score function* $s : \mathcal{Y} \times \mathcal{X} \rightarrow [-1, 1]$, which assigns a *scores*(y_t, x_t). The algorithm \mathcal{A} aims to minimize the *regret*

$$\text{Regret}(T) := \sum_{t=1}^T (s_\star(y_t) - s_{g_t}(y_t)), \quad (4)$$

where we denote by $s_g(y) := \mathbb{E}_{x_g \sim P_g(\cdot | y)}[s(y, x_g)]$ the expected score of any model $g \in \mathcal{G}$ and $s_\star(y) := \max_{g \in \mathcal{G}} s_g(y)$ the optimal expected score, both conditioned on the prompt y .

5 An Optimism-based Approach for Prompt-based Selection

Under the online prompt-based selection setting, a key challenge is to learn the relationship between the prompt and the score of each model. In this paper, we consider kernel methods for score prediction. Specifically, for each model $g \in \mathcal{G}$, we assume the existence of a (possibly non-linear and infinite-dimensional) feature map ϕ and a weight w_g^\star in an RKHS, such that the score $s_g(y)$ conditioned on the prompt y is given by $(\phi(y))^\top w_g^\star$. Notably, the weight vector w_g^\star is arm-specific and can vary across the models, which is stated in the following assumption.

Protocol 1 Online Prompt-based Selection of Generative Models

Require: total iterations $T \in \mathbb{N}_+$, set of generators $\mathcal{G} = [G]$, prompt distribution $\rho \in \Delta(\mathcal{Y})$, score function $s : \mathcal{Y} \times \mathcal{X} \rightarrow [-1, 1]$, algorithm $\mathcal{A} : (\mathcal{Y} \times \mathcal{G} \times \mathbb{R})^* \times \mathcal{Y} \rightarrow \Delta(\mathcal{G})$

Initialize: observation sequence $\mathcal{D} \leftarrow \emptyset$

- 1: **for** iteration $t = 1, 2, \dots, T$ **do**
 - 2: Prompt $y_t \sim \rho$ is revealed.
 - 3: Algorithm \mathcal{A} picks model $g_t \sim \mathcal{A}(\cdot | \mathcal{D}, y_t)$ and samples an answer $x_t \sim P_{g_t}(\cdot | y_t)$.
 - 4: Score $s_t \leftarrow s(y_t, x_t)$ is assigned.
 - 5: Update observation $\mathcal{D} \leftarrow \mathcal{D} \cup \{(y_t, g_t, s_t)\}$.
 - 6: **end for**
-

Assumption 1 (Realizability). *There exists a mapping $\phi : \mathbb{R}^d \rightarrow \mathcal{H}$ and weight $w_g^* \in \mathcal{H}$ such that score $s_g(y) = \langle y, w_g^* \rangle_{\mathcal{H}}$ for any prompt vector $y \in \mathbb{R}^d$ and model $g \in \mathcal{G}$. Further, it holds that $\|w_g^*\| \leq 1$, and $k(y, y) \leq \kappa^2$ and $\|\phi(y)\| \leq 1$ for any $y \in \mathcal{Y}$, where $k : \mathbb{R}^d \times \mathbb{R}^d \rightarrow \mathbb{R}$ is the kernel function of the mapping ϕ .*

Remark 1 (Comparison to linear and kernelized CB). *We note that Assumption 1 differs from the standard settings of linear and kernelized contextual bandit (CB) (Chu et al., 2011; Valko et al., 2013; Zenati et al., 2022). Specifically, in these settings, a different context variable is observed at each arm, and a single weight vector is applied uniformly across all arms. In the prompt-based model selection setting, the text prompt (i.e., the context variable) is shared among arms (i.e., the generative models) and can result in different performance scores across the models, which cannot be captured by the standard kernelized CB approach.*

Remark 2 (Kernelized scores). *Note that the relationship between the prompt vector and score can be non-linear and dependent on the choice of the generative model. For instance, the generated images often vary across the prompts and different T2I models, which will affect the resulting CLIPScore (1).*

5.1 The PAK-UCB Algorithm

In this section, we present PAK-UCB in Algorithm 2, an online learning approach to prompt-based model selection. For each incoming prompt, PAK-UCB first estimates the performance scores via kernel ridge regression (KRR) and then picks the model with the highest estimated score. Unlike standard LinUCB (Chu et al., 2011) and KernelUCB (Valko et al., 2013) algorithms, which train a single reward function shared across all arms, PAK-UCB learns arm-specific functions to predict the score of each model.

The key component in PAK-UCB is the function COMPUTE_UCB (lines 8-17), which outputs both the KRR estimator $\hat{\mu}_g$ and an uncertainty quantifier $\hat{\sigma}_g$. As the weight vector w_g^* can vary across the arms, PAK-UCB constructs the KRR dataset using prompt-score pairs from iterations where model g is chosen, with the corresponding indices stored in the set Ψ_g (line 6). The estimated score is then computed by $\hat{s}_g = \hat{\mu}_g + (2\eta + \sqrt{\alpha})\hat{\sigma}_g$ (line 4), which is initially set to $+\infty$ to ensure each model is picked at least once (lines 9-10). Particularly, the following lemma shows that under some conditions, \hat{s}_g is an optimistic estimation of $s_g(y_t)$ with high probability. The detailed proof can be found in Appendix C.1.

Algorithm 2 Per-Arm Kernelized UCB (PAK-UCB)

Require: total iterations $T \in \mathbb{N}_+$, set of generators $\mathcal{G} = [G]$, prompt distribution $\rho \in \Delta(\mathcal{Y})$, score function $s : \mathcal{Y} \times \mathcal{X} \rightarrow [-1, 1]$, positive definite kernel $k : \mathcal{Y} \times \mathcal{Y} \rightarrow \mathbb{R}$, regularization and exploration parameters $\alpha, \eta \geq 0$

Initialize: observation sequence $\mathcal{D} \leftarrow \emptyset$ and index set $\Psi_g \leftarrow \emptyset$ for all $g \in \mathcal{G}$

```
1: for iteration  $t = 1, 2, \dots, T$  do
2:   Prompt  $y_t \sim \rho$  is revealed.
3:   Compute  $(\hat{\mu}_g, \hat{\sigma}_g) \leftarrow \text{COMPUTE\_UCB}(\mathcal{D}, y_t, \Psi_g)$  for each  $g \in \mathcal{G}$ .
4:   Pick model  $g_t \leftarrow \arg \max_{g \in \mathcal{G}} \{\hat{s}_g\}$ , where  $\hat{s}_g \leftarrow \hat{\mu}_g + (2\eta + \sqrt{\alpha}) \cdot \hat{\sigma}_g$ .
5:   Sample an answer  $x_t \sim P_{g_t}(\cdot | y_t)$  and compute the score  $s_t \leftarrow s(y_t, x_t)$ .
6:   Update  $\mathcal{D} \leftarrow \mathcal{D} \cup \{(y_t, s_t)\}$  and  $\Psi_{g_t} \leftarrow \Psi_{g_t} \cup \{t\}$ .
7: end for

8: function COMPUTE_UCB( $\mathcal{D}, y, \Psi_g$ )
9:   if  $\Psi_g$  is empty then
10:     $\hat{\mu}_g \leftarrow +\infty, \hat{\sigma}_g \leftarrow +\infty$ .
11:   else
12:    Set  $K \leftarrow [k(y_i, y_j)]_{i,j \in \Psi_g}, v \leftarrow [s_i]_{i \in \Psi_g}^\top$ , and  $k_y \leftarrow [k(y, y_i)]_{i \in \Psi_g}^\top$ .
13:     $\hat{\mu}_g \leftarrow k_y^\top (K + \alpha I)^{-1} v$ .
14:     $\hat{\sigma}_g \leftarrow \alpha^{-\frac{1}{2}} \sqrt{k(y, y) - k_y^\top (K + \alpha I)^{-1} k_y}$ .
15:   end if
16:   return  $(\hat{\mu}_g, \hat{\sigma}_g)$ .
17: end function
```

Lemma 1 (Optimism). *Let $\Psi_g \subseteq [T]$ be an index set such that the set of scores $\{s_t : t \in \Psi_g\}$ are independent random variables. Then, under Assumption 1, with probability at least $1 - \delta$, the quantity $\hat{\mu}_g$ computed in function $\text{COMPUTE_UCB}(\mathcal{D}, y, \Psi_g)$ satisfies that*

$$|\hat{\mu}_g - s_g(y)| \leq (2\eta + \sqrt{\alpha})\hat{\sigma}_g, \quad (5)$$

where $\eta = \sqrt{2 \log(2/\delta)}$. Hence, it holds that $\hat{s}_g = \hat{\mu}_g + (2\eta + \sqrt{\alpha})\hat{\sigma}_g \geq s_g(y)$.

We show that a variant of PAK-UCB attains a regret of $\tilde{O}(\sqrt{GT})$. The formal statement and the proof can be found in Appendix A.

Theorem 1 (Regret, informal). *Under the same conditions in Lemma 1, with probability of at least $1 - \delta$, a variant of Algorithm 2 attains a regret of $\tilde{O}(\sqrt{GT})$.*

5.2 PAK-UCB with Random Fourier Features

The PAK-UCB solves a KRR for each model at an iteration to estimate the scores, which can be expensive in both computation and memory for a large number of iterations. To address this problem, we leverage the random Fourier features (RFF) sampling (Rahimi and Recht, 2007b) for positive definite shift-invariant kernels. At a high level, RFF maps the input data, e.g., the prompt (vector) in our setting, to a randomized low-dimensional feature space and then applies fast linear

methods to solve the regression problem. Particularly, the inner product between these projected randomized features is an *unbiased* estimation of the kernel value.

We present the RFF-UCB algorithm, which is a variant of PAK-UCB with random features. RFF-UCB leverages an RFF-based approach to compute the mean and uncertainty quantifier in line 3 of Algorithm 2, which we present in Algorithm 3. Upon receiving the regression dataset consisting of prompt-score pairs, COMPUTE_UCB_RFF first projects each d -dimensional prompt vector to a randomized s -dimensional feature space according to Equation (3) (lines 5-6) and then solves a linear ridge regression to estimate the mean and uncertainty (lines 8-9). To derive statistical guarantees, the number of features varies according to both the input data and error thresholds, which we will specify in Appendix B.1. In practice, we find that a size around 50 can attain satisfactory empirical performance. To see why RFF can reduce the computation, note that the size of the (regularized) Gram matrix $(\tilde{\Phi}_g^\top \tilde{\Phi}_g + \alpha I)$ in line 8 is fixed to be s in the whole process, while the size of $(K + \alpha I)$ in line 13 of Algorithm 2 scales with $|\Psi_g|$ and can grow linearly over iterations. Particularly, the following lemma shows that COMPUTE_UCB_RFF can reduce the time and space by an order of $O(t^2)$ and $O(t)$, respectively.

Algorithm 3 Compute UCB with Random Fourier Features

Require: the Fourier transform p of a positive definite shift-invariant kernel $k(y, y') = k(y - y')$, error thresholds $\epsilon_{\text{RFF}}, \Delta_{\text{RFF}} > 0$, regularization and exploration parameters $\alpha, \eta \geq 0$

Initialize: number of features s , bonus terms $\mathcal{B}_{g,1}$ and $\mathcal{B}_{g,2}$

```

1: function COMPUTE_UCB_RFF( $\mathcal{D}, y, \Psi_g$ )
2:   if  $\Psi_g$  is empty then
3:      $\tilde{\mu}_g \leftarrow +\infty, \tilde{\sigma}_g \leftarrow +\infty$ .
4:   else
5:     Draw  $\omega_1, \dots, \omega_s \stackrel{\text{i.i.d.}}{\sim} p$  and  $b_1, \dots, b_s \stackrel{\text{i.i.d.}}{\sim} \text{Unif}([0, 2\pi])$ .
6:     Define mapping  $\varphi(y') \leftarrow \sqrt{\frac{2}{s}} \cdot [\cos(w_1^\top y + b_1), \dots, \cos(w_s^\top y + b_s)]^\top$  for any  $y' \in \mathbb{R}^d$ .
7:     Set  $\tilde{\Phi}_g \leftarrow [\varphi(y_i)^\top]_{i \in \Psi_g}$  and  $v \leftarrow [s_i]_{i \in \Psi_g}^\top$ .
8:      $\tilde{\mu}_g \leftarrow (\varphi(y))^\top (\tilde{\Phi}_g^\top \tilde{\Phi}_g + \alpha I)^{-1} \tilde{\Phi}_g^\top v + \mathcal{B}_{g,1}$ .
9:      $\tilde{\sigma}_g \leftarrow \alpha^{-\frac{1}{2}} (1 - (\varphi(y))^\top (\tilde{\Phi}_g^\top \tilde{\Phi}_g + \alpha I)^{-1} \tilde{\Phi}_g^\top \tilde{\Phi}_g (\varphi(y)))^{\frac{1}{2}} + \mathcal{B}_{g,2}$ .
10:  end if
11:  return  $(\tilde{\mu}_g, \tilde{\sigma}_g)$ .
12: end function

```

Lemma 2 (Time and space complexity). *At any iteration $t \in [T]$, COMPUTE_UCB (lines 8-17 of Algorithm 2) requires $O(t^3/G^2)$ time and $O(t^2/G)$ space, while COMPUTE_UCB_RFF with random features of size $s \in \mathbb{N}_+$ (Algorithm 3) requires $O(ts^2)$ time and $O(ts)$ space, where G is the number of generators. See Appendix B.5 for details.*

It can be shown that the implementation of PAK-UCB with RFF attains the exact same regret guarantees for adaptively selected feature sizes. The formal statement and the proof can be found in Appendix B.2.

Theorem 2 (Regret when using RFF, informal). *Under the same conditions in Theorem 4, a variant of RFF-UCB attains a regret of $\tilde{O}(\sqrt{GT})$.*

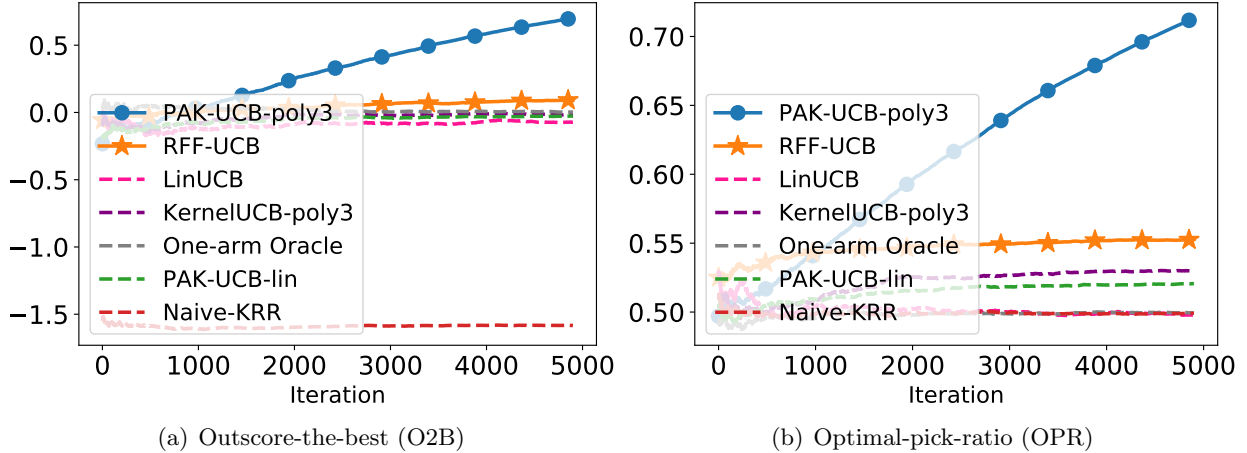


Figure 2: Prompt-based selection between Stable Diffusion v1.5 and PixArt- α (Figure 1(a)): Results are averaged over 20 trials.

6 Numerical Results

In this section, we present numerical results for the proposed 1) **PAK-UCB-poly3** algorithm (PAK-UCB using a polynomial kernel with degree 3, i.e., $k_{\text{poly3}}(x_1, x_2) = (1 + x_1^\top x_2)^3$), and 2) the **RFF-UCB** algorithm with the RBF kernel. Our primary focus is on prompt-based selection among standard text-to-image (T2I) models: Stable Diffusion v1.5¹, PixArt- α -XL-2-512x512², UniDiffuser³, and DeepFloyd IF-I-M-v1.0.⁴. Additionally, we conduct experiments on image captioning (image-to-text) task and video data under synthetic setups. Detailed implementation of the algorithms and additional results can be found in Appendix D.

6.1 Experimental Details

Baselines. We compare PAK-UCB-poly3 and RFF-UCB with five baselines, including 1) **LinUCB** and **KernelUCB-poly3**: standard LinUCB (Chu et al., 2011) and KernelUCB (Valko et al., 2013) using a polynomial kernel with degree 3, where the context variable of each arm is given by the concatenation of the CLIP embedding of the text prompt and its one-hot indicator vector, 2) **One-arm Oracle**: always picking the model with the maximum averaged CLIPScore, 3) **PAK-UCB-lin**: PAK-UCB with linear kernel, i.e., $k_{\text{lin}}(x_1, x_2) = x_1^\top x_2$, which does not incorporate non-linearity in score estimation, and 4) **Naive-KRR**: PAK-UCB-poly3 without exploration, which selects the model with the highest estimated mean conditioned to the prompt.

Performance metrics. For each experiment, we report two performance metrics: (i) *outscore-the-best* (O2B): the difference between the CLIPScore attained by the algorithm and the highest average CLIPScore attained by any single model, and (ii) *optimal-pick-ratio* (OPR): the overall ratio that the algorithm picks the best generator conditioned to the prompt type.

¹https://huggingface.co/docs/diffusers/en/api/pipelines/stable_diffusion/text2img

²<https://huggingface.co/PixArt-alpha/PixArt-XL-2-512x512>

³<https://github.com/thu-ml/unidiffuser>

⁴<https://github.com/deep-floyd/IF>

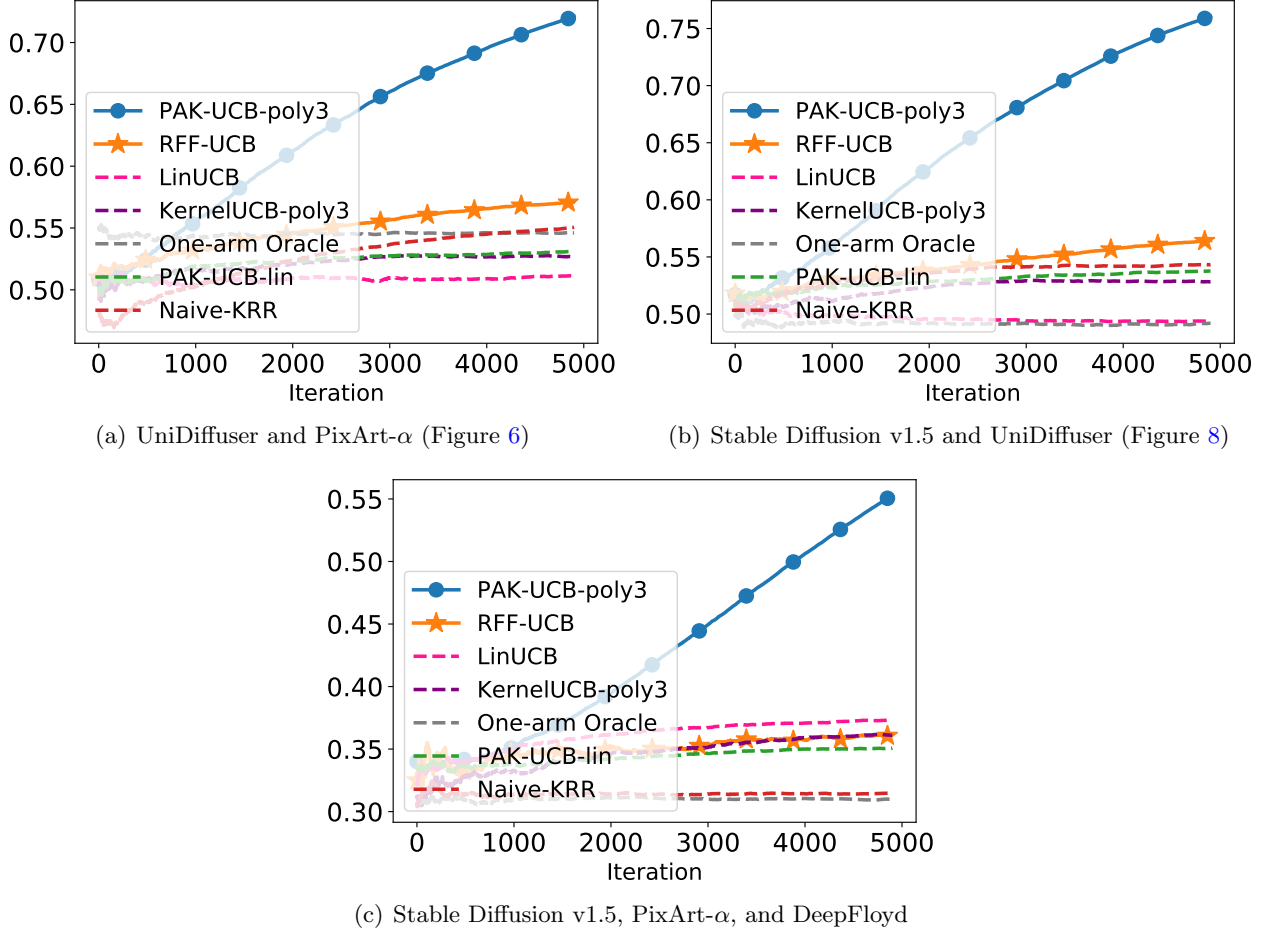


Figure 3: Prompt-based selection among several standard T2I models: Optimal-pick-ratio (OPR) is reported. The selection of our proposed PAK-UCB-poly3 algorithm converges quickly to the optimal model for incoming text prompts. Results for Outscore-the-best (O2B) can be found in Figures 7, 9, and 10 in the Appendix. Results are averaged over 20 trials.

6.2 Summary

The main finding of our numerical experiments is the improvement of the proposed contextual bandit PAK-UCB algorithm over the one-arm oracle baseline. This result means that the online learning algorithm can outperform a user with side-knowledge of the single best-performing model, which is made possible by a *prompt-based selection* of the model. This finding supports the application of contextual bandit algorithms in the selection of text-based generative models. Moreover, our numerical results indicate that the proposed PAK-UCB algorithm can significantly outperform the standard LinUCB (Chu et al., 2011) and KernelUCB (Valko et al., 2013) methods, showcasing the effectiveness of our framework in the prompt-based model selection setting. Additionally, the proposed PAK-UCB algorithm can perform better with a non-linear kernel function. Finally, in our experiments, the proposed RFF-UCB variant could reduce the computational costs of the general PAK-UCB algorithm.

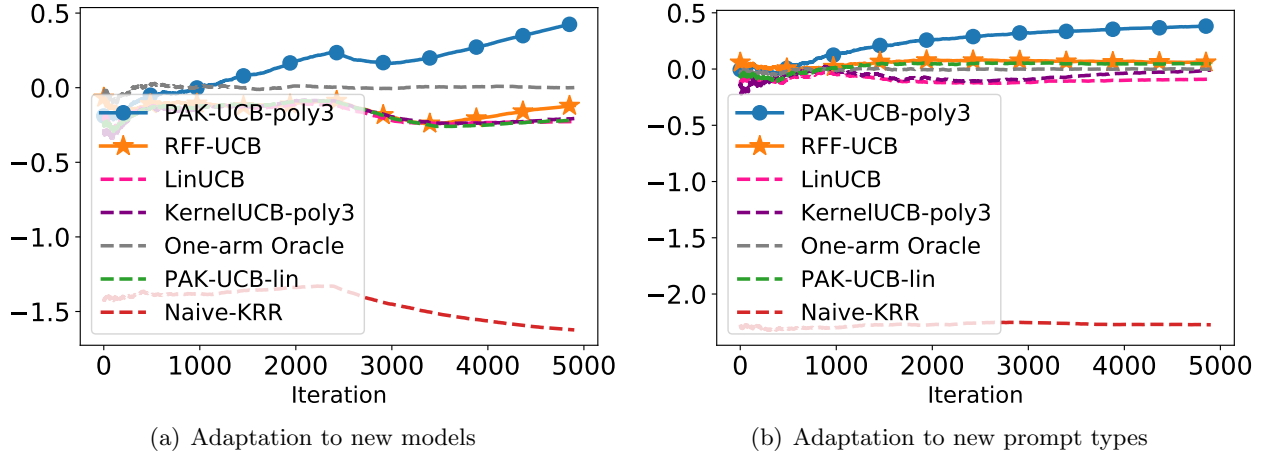


Figure 4: Adaptation to new models and prompt types: Outscore-the-best (O2B) is reported. Results for Optimal-pick-ratio (OPR) can be found in Figures 11 and 12 in the Appendix. Results are averaged over 20 trials.

6.3 Experimental Setups

Setup 1. Prompt-based selection among standard text-to-image models. The first set of experiments are on the setup illustrated in Figure 1(a), where we generate images from Stable Diffusion v1.5 and PixArt- α . The results show that PAK-UCB-poly3 outperforms the baseline algorithm and attains a high optimal-pick-ratio, which shows that it can identify the optimal model conditioned to the prompt (see Figure 2). Additionally, we provide numerical results on various T2I generative models, including UniDiffuser and DeepFloyd (see Figure 3).

Setup 2. Adaptation to new prompt types and models. We consider scenarios where new text-to-image models or prompt types are introduced after the initial deployment. At the beginning of the first experiment, Stable Diffusion v1.5 and PixArt- α are available, and UniDiffuser is introduced after 2500 iterations. In the second experiment, we generate samples from both PixArt- α and UniDiffuser, and a new prompt type is introduced after each 1000 iterations. The results show that PAK-UCB-poly3 can well adapt to new prompt types and generators (see Figure 11).

Setup 3. Synthetic experiments on other conditional generation tasks. We provide numerical results on image-captioning (image-to-text) and text-to-video (T2V) task under synthetic setups. The details can be found in Appendix D.

7 Conclusion

In this work, we investigated prompt-based selection of generative models using a contextual bandit algorithm, which can identify the best available generative model for a given text prompt. We propose two kernel-based algorithms, including PAK-UCB and RFF-UCB, to perform this selection task. Our numerical results on text-to-image, text-to-video, and image-captioning tasks demonstrate the effectiveness of the proposed framework in scenarios where the available generative models have varying performance rankings depending on the type of prompt. An interesting

direction for future research is to extend the application of our algorithms to text-to-text language models, where different models may respond better to questions on different topics. Furthermore, considering evaluation criteria beyond relevance, such as diversity and novelty scores, could lead to extensions of our proposed framework.

References

- Astolfi, P., Careil, M., Hall, M., Mañas, O., Muckley, M., Verbeek, J., Soriano, A. R., and Drozdal, M. (2024). Consistency-diversity-realism pareto fronts of conditional image generative models.
- Auer, P. (2003). Using confidence bounds for exploitation-exploration trade-offs. *J. Mach. Learn. Res.*, 3(null):397–422.
- Avron, H., Kapralov, M., Musco, C., Musco, C., Velingker, A., and Zandieh, A. (2017). Random Fourier features for kernel ridge regression: Approximation bounds and statistical guarantees. In Precup, D. and Teh, Y. W., editors, *Proceedings of the 34th International Conference on Machine Learning*, volume 70 of *Proceedings of Machine Learning Research*, pages 253–262. PMLR.
- Bao, F., Nie, S., Xue, K., Cao, Y., Li, C., Su, H., and Zhu, J. (2023). All are worth words: A vit backbone for diffusion models. In *CVPR*.
- Calandriello, D., Carratino, L., Lazaric, A., Valko, M., and Rosasco, L. (2019). Gaussian process optimization with adaptive sketching: Scalable and no regret. In Beygelzimer, A. and Hsu, D., editors, *Proceedings of the Thirty-Second Conference on Learning Theory*, volume 99 of *Proceedings of Machine Learning Research*, pages 533–557. PMLR.
- Calandriello, D., Carratino, L., Lazaric, A., Valko, M., and Rosasco, L. (2020). Near-linear time Gaussian process optimization with adaptive batching and resparsification. In III, H. D. and Singh, A., editors, *Proceedings of the 37th International Conference on Machine Learning*, volume 119 of *Proceedings of Machine Learning Research*, pages 1295–1305. PMLR.
- Cherti, M., Beaumont, R., Wightman, R., Wortsman, M., Ilharco, G., Gordon, C., Schuhmann, C., Schmidt, L., and Jitsev, J. (2023). Reproducible scaling laws for contrastive language-image learning. In *Proceedings of the IEEE/CVF Conference on Computer Vision and Pattern Recognition*, pages 2818–2829.
- Chu, W., Li, L., Reyzin, L., and Schapire, R. (2011). Contextual bandits with linear payoff functions. In Gordon, G., Dunson, D., and Dudík, M., editors, *Proceedings of the Fourteenth International Conference on Artificial Intelligence and Statistics*, volume 15 of *Proceedings of Machine Learning Research*, pages 208–214, Fort Lauderdale, FL, USA. PMLR.
- Ding, M., Yang, Z., Hong, W., Zheng, W., Zhou, C., Yin, D., Lin, J., Zou, X., Shao, Z., Yang, H., and Tang, J. (2021). Cogview: Mastering text-to-image generation via transformers. In Ranzato, M., Beygelzimer, A., Dauphin, Y., Liang, P., and Vaughan, J. W., editors, *Advances in Neural Information Processing Systems*, volume 34, pages 19822–19835. Curran Associates, Inc.
- Foster, D., Agarwal, A., Dudik, M., Luo, H., and Schapire, R. (2018). Practical contextual bandits with regression oracles. In Dy, J. and Krause, A., editors, *Proceedings of the 35th International*

- Conference on Machine Learning*, volume 80 of *Proceedings of Machine Learning Research*, pages 1539–1548. PMLR.
- Hessel, J., Holtzman, A., Forbes, M., Le Bras, R., and Choi, Y. (2021). CLIPScore: A reference-free evaluation metric for image captioning. In Moens, M.-F., Huang, X., Specia, L., and Yih, S. W.-t., editors, *Proceedings of the 2021 Conference on Empirical Methods in Natural Language Processing*, pages 7514–7528, Online and Punta Cana, Dominican Republic. Association for Computational Linguistics.
- Heusel, M., Ramsauer, H., Unterthiner, T., Nessler, B., and Hochreiter, S. (2017). Gans trained by a two time-scale update rule converge to a local nash equilibrium. *Advances in neural information processing systems*, 30.
- Huang, R., Huang, J., Yang, D., Ren, Y., Liu, L., Li, M., Ye, Z., Liu, J., Yin, X., and Zhao, Z. (2023). Make-an-audio: Text-to-audio generation with prompt-enhanced diffusion models. In Krause, A., Brunskill, E., Cho, K., Engelhardt, B., Sabato, S., and Scarlett, J., editors, *Proceedings of the 40th International Conference on Machine Learning*, volume 202 of *Proceedings of Machine Learning Research*, pages 13916–13932. PMLR.
- Huang, Z., He, Y., Yu, J., Zhang, F., Si, C., Jiang, Y., Zhang, Y., Wu, T., Jin, Q., Chanpaisit, N., Wang, Y., Chen, X., Wang, L., Lin, D., Qiao, Y., and Liu, Z. (2024). VBench: Comprehensive benchmark suite for video generative models. In *Proceedings of the IEEE/CVF Conference on Computer Vision and Pattern Recognition*.
- Kannen, N., Ahmad, A., Andreetto, M., Prabhakaran, V., Prabhu, U., Dieng, A. B., Bhattacharyya, P., and Dave, S. (2024). Beyond aesthetics: Cultural competence in text-to-image models.
- Kim, J.-H., Kim, Y., Lee, J., Yoo, K. M., and Lee, S.-W. (2022). Mutual information divergence: A unified metric for multimodal generative models. In Oh, A. H., Agarwal, A., Belgrave, D., and Cho, K., editors, *Advances in Neural Information Processing Systems*.
- Kirstain, Y., Polyak, A., Singer, U., Matiana, S., Penna, J., and Levy, O. (2023). Pick-a-pic: An open dataset of user preferences for text-to-image generation. In *Thirty-seventh Conference on Neural Information Processing Systems*.
- Langford, J. and Zhang, T. (2007). The epoch-greedy algorithm for multi-armed bandits with side information. In Platt, J., Koller, D., Singer, Y., and Roweis, S., editors, *Advances in Neural Information Processing Systems*, volume 20. Curran Associates, Inc.
- Li, L., Chu, W., Langford, J., and Schapire, R. E. (2010). A contextual-bandit approach to personalized news article recommendation. In *Proceedings of the 19th International Conference on World Wide Web, WWW ’10*, page 661–670, New York, NY, USA. Association for Computing Machinery.
- Masrourisaadat, N., Sedaghatkish, N., Sarshartehrani, F., and Fox, E. A. (2024). Analyzing quality, bias, and performance in text-to-image generative models.
- Pan, Y., Qiu, Z., Yao, T., Li, H., and Mei, T. (2018). To create what you tell: Generating videos from captions.

- Peng, Y., Cui, Y., Tang, H., Qi, Z., Dong, R., Bai, J., Han, C., Ge, Z., Zhang, X., and Xia, S.-T. (2024). Dreambench++: A human-aligned benchmark for personalized image generation.
- Podell, D., English, Z., Lacey, K., Blattmann, A., Dockhorn, T., Müller, J., Penna, J., and Rombach, R. (2024). SDXL: Improving latent diffusion models for high-resolution image synthesis. In *The Twelfth International Conference on Learning Representations*.
- Radford, A., Kim, J. W., Hallacy, C., Ramesh, A., Goh, G., Agarwal, S., Sastry, G., Askell, A., Mishkin, P., Clark, J., Krueger, G., and Sutskever, I. (2021a). Learning transferable visual models from natural language supervision.
- Radford, A., Kim, J. W., Hallacy, C., Ramesh, A., Goh, G., Agarwal, S., Sastry, G., Askell, A., Mishkin, P., Clark, J., Krueger, G., and Sutskever, I. (2021b). Learning transferable visual models from natural language supervision. In Meila, M. and Zhang, T., editors, *Proceedings of the 38th International Conference on Machine Learning*, volume 139 of *Proceedings of Machine Learning Research*, pages 8748–8763. PMLR.
- Rahimi, A. and Recht, B. (2007a). Random features for large-scale kernel machines. *Advances in neural information processing systems*, 20.
- Rahimi, A. and Recht, B. (2007b). Random features for large-scale kernel machines. In Platt, J., Koller, D., Singer, Y., and Roweis, S., editors, *Advances in Neural Information Processing Systems*, volume 20. Curran Associates, Inc.
- Reed, S., Akata, Z., Yan, X., Logeswaran, L., Schiele, B., and Lee, H. (2016). Generative adversarial text to image synthesis. In Balcan, M. F. and Weinberger, K. Q., editors, *Proceedings of The 33rd International Conference on Machine Learning*, volume 48 of *Proceedings of Machine Learning Research*, pages 1060–1069, New York, New York, USA. PMLR.
- Rudin, W. (2017). *Fourier analysis on groups*. Courier Dover Publications.
- Salimans, T., Goodfellow, I., Zaremba, W., Cheung, V., Radford, A., Chen, X., and Chen, X. (2016). Improved techniques for training GANs. In Lee, D., Sugiyama, M., Luxburg, U., Guyon, I., and Garnett, R., editors, *Advances in Neural Information Processing Systems*, volume 29. Curran Associates, Inc.
- Singer, U., Polyak, A., Hayes, T., Yin, X., An, J., Zhang, S., Hu, Q., Yang, H., Ashual, O., Gafni, O., Parikh, D., Gupta, S., and Taigman, Y. (2022). Make-a-video: Text-to-video generation without text-video data.
- Tan, Z., Yang, X., Qin, L., Yang, M., Zhang, C., and Li, H. (2024). Evalalign: Supervised fine-tuning multimodal llms with human-aligned data for evaluating text-to-image models.
- Valko, M., Korda, N., Munos, R., Flaounas, I., and Cristianini, N. (2013). Finite-time analysis of kernelised contextual bandits.
- Xu, J., Mei, T., Yao, T., and Rui, Y. (2016). Msr-vtt: A large video description dataset for bridging video and language. In *2016 IEEE Conference on Computer Vision and Pattern Recognition (CVPR)*, pages 5288–5296.

- Xu, T., Zhang, P., Huang, Q., Zhang, H., Gan, Z., Huang, X., and He, X. (2018). AttnGAN: Fine-grained text to image generation with attentional generative adversarial networks. In *Proceedings of the IEEE Conference on Computer Vision and Pattern Recognition (CVPR)*.
- Zenati, H., Bietti, A., Diemert, E., Mairal, J., Martin, M., and Gaillard, P. (2022). Efficient kernelized ucb for contextual bandits. In Camps-Valls, G., Ruiz, F. J. R., and Valera, I., editors, *Proceedings of The 25th International Conference on Artificial Intelligence and Statistics*, volume 151 of *Proceedings of Machine Learning Research*, pages 5689–5720. PMLR.

A Proof in Section 5.1

The technical challenge in analyzing PAK-UCB is that predictions in later iterations make use of previous outcomes. Hence, the rewards $\{s_i\}_{i \in \Psi_g}$ are not independent if the index set Φ_g is updated each time when model g is chosen (line 6 of Algorithm 2). To address this problem, we leverage a standard approach used in prior works (Auer, 2003; Chu et al., 2011; Valko et al., 2013) and present a variant of PAK-UCB in Algorithm 4, which is called Sup-PAK-UCB. We prove it attains a regret of order $\tilde{O}(\sqrt{T})$.

A.1 The Sup-PAK-UCB Algorithm

Algorithm 4 Sup-PAK-UCB

Require: total iterations $T \in \mathbb{N}_+$, set of generators $\mathcal{G} = [G]$, prompt distribution $\rho \in \Delta(\mathcal{Y})$, score function $s : \mathcal{Y} \times \mathcal{X} \rightarrow [-1, 1]$, positive definite kernel $k : \mathcal{Y} \times \mathcal{Y} \rightarrow \mathbb{R}$, regularization and exploration parameters $\alpha, \eta \geq 0$, function COMPUTE_UCB in Algorithm 2

Initialize: observation sequence $\mathcal{D} \leftarrow \emptyset$ and index sets $\{\Psi_g^m \leftarrow \emptyset\}_{m=1}^M$ for all $g \in \mathcal{G}$, where $M \leftarrow \log T$

```

1: for iteration  $t = 1, 2, \dots, T$  do
2:   Prompt  $y_t \sim \rho$  is revealed.
3:   Set stage  $m \leftarrow 1$  and  $\hat{\mathcal{G}}^1 \leftarrow \mathcal{G}$ .
4:   repeat
5:     Compute  $\{(\hat{\mu}_g^m, \hat{\sigma}_g^m) \leftarrow \text{COMPUTE\_UCB}(\mathcal{D}, y_t, \Psi_g^m)\}_{g \in \hat{\mathcal{G}}^m}$ .
6:     Set upper confidence bound  $\hat{s}_g^m(y) \leftarrow \hat{\mu}_g^m + (2\eta + \sqrt{\alpha}) \cdot \hat{\sigma}_g^m$  for all  $g \in \hat{\mathcal{G}}^m$ .
7:     if  $(2\eta + \sqrt{\alpha}) \cdot \hat{\sigma}_g^m \leq 1/\sqrt{T}$  for all  $g \in \hat{\mathcal{G}}^m$  then
8:       Pick model  $g_t \leftarrow \arg \max \hat{s}_g^m(y)$ .
9:     else if  $(2\eta + \sqrt{\alpha}) \cdot \hat{\sigma}_g^m \leq 2^{-m}$  for all  $g \in \hat{\mathcal{G}}^m$  then
10:       $\hat{\mathcal{G}}^{m+1} \leftarrow \{g \in \hat{\mathcal{G}}^m : \hat{s}_g^m(y) \geq \max_{g \in \hat{\mathcal{G}}^m} \hat{s}_g^m(y) - 2^{1-m}\}$ .
11:      Set stage  $m \leftarrow m + 1$ .
12:     else
13:       Pick  $g_t \in \hat{\mathcal{G}}^m$  such that  $(2\eta + \sqrt{\alpha}) \cdot \hat{\sigma}_{g_t}^m > 2^{-m}$ .
14:       Update  $\Psi_{g_t}^m \leftarrow \Psi_{g_t}^m \cup \{t\}$ .
15:     end if
16:   until a model  $g_t$  is selected
17:   Sample an answer  $x_t \sim P_{g_t}(\cdot | y_t)$  and compute the score  $s_t \leftarrow s(y_t, x_t)$ .
18:   Update  $\mathcal{D} \leftarrow \mathcal{D} \cup \{(y_t, s_t)\}$ .
19: end for

```

A.2 Analysis

In this section, we prove the following regret bound of Sup-PAK-UCB.

Theorem 3 (Regret of Sup-PAK-UCB). *Under Assumption 1, with probability at least $1 - \delta$, the*

regret of Sup-PAK-UCB with $\eta = \sqrt{2\log(2(\log T)GT/\delta)}$ is bounded by

$$\text{Regret}(T) \leq \tilde{O} \left((1 + \sqrt{\alpha}) \sqrt{d_{\text{eff}} \left(10 + \frac{15}{\alpha} \right) GT} \right) \quad (6)$$

where d_{eff} is a data-dependent quantity defined in Lemma 10 and logarithmic factors are hidden in the notation $\tilde{O}(\cdot)$.

Notations. To facilitate the analysis, we add an subscript t to all the notations in Algorithm 4 to indicate they are quantities computed at the t -th iteration, i.e., $\hat{\mu}_{g,t}^m, \hat{\sigma}_{g,t}^m, \hat{s}_{g,t}^m, \hat{\mathcal{G}}_t^m$, and $\Psi_{g,t}^m$.⁵

We leverage the following two lemmas to prove Theorem 3. The first lemma shows that the construction of index sets $\{\Psi_{g,t}^m\}_{m=1}^M$ ensures the independence among the rewards $\{s_i\}_{i \in \Psi_{g,t}^m}$, which allows us to utilize Lemma 1 to bound the estimation error.

Lemma 3 (Auer (2003), Lemma 14). *For any iteration $t \in [T]$, model $g \in \mathcal{G}$, and stage $m \in [M]$, the set of rewards $\{s_i\}_{i \in \Psi_{g,t}^m}$ are independent random variables such that $\mathbb{E}[s_i] = s_g(y_i)$.*

The second lemma shows several properties of the estimated score $\hat{s}_{g,t}^m$ and the set $\hat{\mathcal{G}}_t^m$. The detailed proof can be found in Appendix C.2.

Lemma 4 (Valko et al. (2013), Lemma 7). *With probability at least $1 - (MGT)\delta$, for any iteration $t \in [T]$ and stage $m \in [M]$, the following hold:*

- $|\hat{\mu}_{g,t}^m - s_g(y_t)| \leq (2\eta + \sqrt{\alpha})\hat{\sigma}_{g,t}^m$ for any $g \in \hat{\mathcal{G}}_t^m$,
- $\arg \max_{g \in \mathcal{G}} s_g(y_t) \in \hat{\mathcal{G}}_t^m$, and
- $s_\star(y_t) - s_g(y_t) \leq 2^{3-m}$ for any $g \in \hat{\mathcal{G}}_t^m$.

Now, we are ready to finish the proof of Theorem 3.

Proof of Theorem 3. Let $\mathcal{T}_1 := \cup_{m \in [M], g \in \mathcal{G}} \Psi_{g,T+1}^m$ and $\mathcal{T}_0 := [T] \setminus \mathcal{T}_1$. Note that \mathcal{T}_0 and \mathcal{T}_1 are sets of iterations such that the model is selected in lines 8 and 13 of Algorithm 4, respectively.

1. Regret incurred in \mathcal{T}_0 . For any $t \in [T]$, let m_t denote the stage that model g_t is picked at the t -th iteration. We have that

$$\begin{aligned} \sum_{t \in \mathcal{T}_0} (s_\star(y_t) - s_{g_t}(y_t)) &\leq \sum_{t \in \mathcal{T}_0} (\hat{s}_{g_\star, t}^{m_t}(y) - s_{g_t}(y_t)) \\ &\leq \sum_{t \in \mathcal{T}_0} (\hat{s}_{g_t, t}^{m_t}(y) - s_{g_t}(y_t)) \\ &= \sum_{t \in \mathcal{T}_0} (\hat{\mu}_{g_t, t}^{m_t} + (2\eta + \sqrt{\alpha})\hat{\sigma}_{g_t, t}^{m_t} - s_{g_t}(y_t)) \\ &\leq 2(2\eta + \sqrt{\alpha}) \sum_{t \in \mathcal{T}_0} \hat{\sigma}_{g_t, t}^{m_t} \\ &\leq 2(2\eta + \sqrt{\alpha}) \sum_{t \in \mathcal{T}_0} T^{-\frac{1}{2}} \leq 2(2\eta + \sqrt{\alpha})\sqrt{T}, \end{aligned} \quad (7)$$

⁵Note that line 14 in the algorithm is rewritten as “ $\Psi_{g_t, t+1}^m \leftarrow \Psi_{g_t, t+1}^m \cup \{t\}$, $\Psi_{g_t, t+1}^{m'} \leftarrow \Psi_{g_t, t}^{m'}$ for any $m' \neq m$, and $\Psi_{g, t+1}^{m'} \leftarrow \Psi_{g, t}^{m'}$ for any $g \neq g_t$ and $m \in [M]$ ”. In addition, we set $\Psi_{g, t+1}^m \leftarrow \Psi_{g, t+1}^m$ for all $g \in \mathcal{G}$ and $m \in [M]$ in line 8.

where the second inequality holds by the definition of g_t and the fact that $g_{\star,t} \in \widehat{\mathcal{G}}_t^{m_t}$, and the fifth inequality holds by line 7 of Algorithm 4.

2. Regret incurred in \mathcal{T}_1 .

$$\begin{aligned} \sum_{t \in \mathcal{T}_1} (s_{\star}(y_t) - s_{g_t}(y_t)) &= \sum_{g \in \mathcal{G}} \sum_{m \in [M]} \sum_{t \in \Psi_{g,T+1}^m} (s_{\star}(y_t) - s_{g_t}(y_t)) \\ &\leq \sum_{g \in \mathcal{G}} \sum_{m \in [M]} 2^{3-m} \cdot |\Psi_{g,T+1}^m|, \end{aligned} \quad (8)$$

where the inequality holds by the last statement in Lemma 4. It remains to bound $|\Psi_{g,T+1}^m|$. First note that for any $m \in [M]$, we have that

$$(2\eta + \sqrt{\alpha}) \sum_{t \in \Psi_{g,T+1}^m} \widehat{\sigma}_{g,t}^m > 2^{-m} \cdot |\Psi_{g,T+1}^m|$$

from line 13 of Algorithm 4. In addition, by a similar statement of (Valko et al., 2013, Lemma 4), which is stated in Lemma 10, we have that

$$\sum_{t \in \Psi_{g,T+1}^m} \widehat{\sigma}_{g,t}^m \leq \widetilde{O} \left(\sqrt{d_{\text{eff}} \left(10 + \frac{15}{\alpha} \right) |\Psi_{g,T+1}^m|} \right), \quad (9)$$

where d_{eff} is defined therein and logarithmic factors are hidden in the notation $\widetilde{O}(\cdot)$. Plugging in Equation (8) results in

$$\begin{aligned} \sum_{t \in \mathcal{T}_1} (s_{\star}(y_t) - s_{g_t}(y_t)) &\leq \widetilde{O} \left((1 + \sqrt{\alpha}) \sum_{g \in \mathcal{G}} \sum_{m \in [M]} \sqrt{d_{\text{eff}} \left(10 + \frac{15}{\alpha} \right) |\Psi_{g,T+1}^m|} \right) \\ &\leq \widetilde{O} \left((1 + \sqrt{\alpha}) \sqrt{GM} \sqrt{d_{\text{eff}} \left(10 + \frac{15}{\alpha} \right) \sum_{g \in \mathcal{G}} \sum_{m \in [M]} |\Psi_{g,T+1}^m|} \right) \\ &\leq \widetilde{O} \left((1 + \sqrt{\alpha}) \sqrt{d_{\text{eff}} \left(10 + \frac{15}{\alpha} \right) GT} \right), \end{aligned} \quad (10)$$

where the second inequality holds by Cauchy-Schwarz inequality.

3. Putting everything together.

Combining Inequalities (7) and (10) leads to

$$\text{Regret}(T) = \left(\sum_{t \in \mathcal{T}_0} + \sum_{t \in \mathcal{T}_1} \right) (s_{\star}(y_t) - s_{g_t}(y_t)) \leq \widetilde{O} \left((1 + \sqrt{\alpha}) \sqrt{d_{\text{eff}} \left(10 + \frac{15}{\alpha} \right) GT} \right),$$

which concludes the proof. \square

B Proof in Section 5.2

B.1 Error of KRR estimators with Random Features

Theorem 4. Assume the error thresholds input to Algorithm 3 satisfy that $\Delta_{\text{RFF}}, \epsilon_{\text{RFF}} \leq 1/2$. Under the same conditions in Lemma 1, with probability at least $1 - 2\delta$, the quantity $\tilde{\mu}_g$ computed by function COMPUTE_UCB_RFF satisfies that

$$|\tilde{\mu}_g - s_g(y)| \leq \mathcal{B}_{g,1} + (2\eta + \sqrt{\alpha})(\tilde{\sigma}_g + \mathcal{B}_{g,2}),$$

with the number of features satisfying Inequality (12) and bonus terms $\mathcal{B}_{g,1}$ and $\mathcal{B}_{g,2}$ given by Equations (11) and (13), where $\eta = \sqrt{2\log(2/\delta)}$. Hence, it holds that $\tilde{s}_g = \tilde{\mu}_g + \mathcal{B}_{g,1} + (2\eta + \sqrt{\alpha})(\tilde{\sigma}_g + \mathcal{B}_{g,2}) \geq s_g(y)$.

Proof. The proof is based on the following two lemmas, which analyze the concentration error of the quantities $\tilde{\mu}_g$ and $\tilde{\sigma}_g$. The detailed proof can be found in Appendix B.3 and B.4, respectively.

Lemma 5 (Concentration of mean using RFF). Let $\Delta_{\text{RFF}}, \epsilon_{\text{RFF}} \leq 1/2$. Under the same conditions in Lemma 1, with probability at least $1 - \delta$, the quantity $\tilde{\mu}_g$ computed by function COMPUTE_UCB_RFF satisfies that

$$|\tilde{\mu}_g - \hat{\mu}_g| \leq \mathcal{B}_{g,1} := \alpha^{-1} |\Psi_g| \epsilon_{\text{RFF}} + \alpha^{-2} \Delta_{\text{RFF}} (\|K\|_2 + \alpha) \quad (11)$$

with the number of features

$$s \geq \max \left\{ \frac{4(d+2)}{\epsilon_{\text{RFF}}^2} \log \left(\frac{\sigma_p^2}{(\delta/2) \cdot \epsilon_{\text{RFF}}^2} \cdot 2^8 \right), \frac{8|\Psi_g|}{3\alpha} \Delta_{\text{RFF}}^{-2} \log \left(\frac{32s_\alpha(K)}{\delta} \right) \right\}, \quad (12)$$

where $\hat{\mu}_g = (\phi(y))^\top \Phi_g^\top (K + \alpha I)^{-1} v$, and σ_p^2 and $s_\alpha(\cdot)$ are two quantities defined in Lemmas 8 and 9, respectively.

Lemma 6 (Concentration of variance using RFF). Let $c > 0$ denote a lower bound of $1 - \|k_y\|_{(K+\alpha I)^{-1}}^2$. Then, conditioned on the successful events in Lemma 5, the quantity $\tilde{\sigma}_g$ computed by function COMPUTE_UCB_RFF satisfies that

$$|\tilde{\sigma}_g - \hat{\sigma}_g| \leq \mathcal{B}_{g,2} := (c \cdot \alpha)^{-\frac{1}{2}} (2|\Psi_g| \alpha^{-2} \Delta_{\text{RFF}} (\|K\|_2 + \alpha) + 3\alpha^{-1} |\Psi_g| \epsilon_{\text{RFF}}) \quad (13)$$

where $\hat{\sigma}_g = \alpha^{-\frac{1}{2}} \sqrt{k(y, y) - k_y^\top (K + \alpha I)^{-1} k_y}$.

Finally, combining Lemmas 1, 5, and 6, we derive that

$$\begin{aligned} |\tilde{\mu}_g - s_g(y)| &\leq |\tilde{\mu}_g - \hat{\mu}_g| + |\hat{\mu}_g - s_g(y)| \\ &\leq \mathcal{B}_{g,1} + (2\eta + \sqrt{\alpha}) \hat{\sigma}_g \\ &\leq \mathcal{B}_{g,1} + (2\eta + \sqrt{\alpha})(\tilde{\sigma}_g + \mathcal{B}_{g,2}), \end{aligned}$$

which concludes the proof. \square

B.2 Sup-PAK-UCB with Random Fourier Features

Algorithm description. To apply RFF to Sup-PAK-UCB, we replace function COMPUTE_UCB with COMPUTE_UCB_RFF in Algorithm 4. To achieve the regret bound (6), an important problem is to design (adaptive) error thresholds, i.e., ϵ_{RFF} and Δ_{RFF} , when computing UCB at each stage m and iteration t . We prove the regret bound in the following theorem.

Theorem 5 (Regret of Sup-RFF-UCB). *Under Assumption 1, with probability at least $1 - \delta$, Sup-RFF-UCB attains the regret bound (6), where $\eta = \sqrt{2 \log(4(\log T)GT/\delta)}$ and sequence of error thresholds input to function COMPUTE_UCB_RFF satisfying Equation (14).*

Proof. The proof is similar to the proof of Theorem 3. First, combining Lemmas 8 and 3, the following lemma can be proved by the exact same analysis for Lemma 4.

Lemma 7. *With probability at least $1 - (2MGT)\delta$, for any iteration $t \in [T]$ and stage $m \in [M]$, the following hold:*

- $|\tilde{\mu}_{g,t}^m - s_g(y_t)| \leq \mathcal{B}_{g,1,t}^m + (2\eta + \sqrt{\alpha})(\tilde{\sigma}_{g,t}^m + \mathcal{B}_{g,2,t}^m)$ for any $g \in \hat{\mathcal{G}}_t^m$,
- $\arg \max_{g \in \mathcal{G}} s_g(y_t) \in \hat{\mathcal{G}}_t^m$, and
- $s_\star(y_t) - s_g(y_t) \leq 2^{3-m}$ for any $g \in \hat{\mathcal{G}}_t^m$.

where the first statement is guaranteed by Theorem 4, $\mathcal{B}_{g,1,t}^m$ and $\mathcal{B}_{g,2,t}^m$ are the bonus (11) and (13) computed at the m -th stage of iteration t .

Next, for iterations in \mathcal{T}_0 (model g_t is picked in line 8 of Algorithm 4), we still have

$$\sum_{t \in \mathcal{T}_0} (s_\star(y_t) - s_{g_t}(y_t)) \leq \tilde{O}(\sqrt{\alpha T}).$$

Further, for iterations in \mathcal{T}_1 (model g_t is picked in line 13 of Algorithm 4), the third statement in the above lemma and line 14 of Algorithm 3 ensure that

$$\begin{aligned} & \sum_{t \in \mathcal{T}_1} (s_\star(y_t) - s_{g_t}(y_t)) \\ & \leq \sum_{g \in \mathcal{G}} \sum_{m \in [M]} 2^{3-m} \cdot |\Psi_{g,T+1}^m| \\ & < 8 \sum_{g \in \mathcal{G}} \sum_{m \in [M]} \sum_{t \in \Psi_{g,T+1}^m} \left(\mathcal{B}_{g_t,1,t}^{m_t} + (2\eta + \sqrt{\alpha})(\tilde{\sigma}_{g,t}^m + \mathcal{B}_{g_t,2,t}^{m_t}) \right) \\ & \leq 8 \sum_{g \in \mathcal{G}} \sum_{m \in [M]} \sum_{t \in \Psi_{g,T+1}^m} \left(\mathcal{B}_{g_t,1,t}^{m_t} + (2\eta + \sqrt{\alpha})(\hat{\sigma}_{g,t}^m + 2\mathcal{B}_{g_t,2,t}^{m_t}) \right) \\ & = 8 \sum_{g \in \mathcal{G}} \sum_{m \in [M]} \left(\sum_{t \in \Psi_{g,T+1}^m} \left(\mathcal{B}_{g_t,1,t}^{m_t} + 2(2\eta + \sqrt{\alpha})\mathcal{B}_{g_t,2,t}^{m_t} \right) + (2\eta + \sqrt{\alpha}) \sum_{t \in \Psi_{g,T+1}^m} \hat{\sigma}_{g,t}^m \right). \end{aligned}$$

Note that the upper bound of the second term has been derived in Equation (9). It remains to bound the first term. Essentially, we will find a sequence of error thresholds, and hence the

number of features defined in Inequality (12), such that the first term is bounded by $\tilde{O}(\sqrt{GT})$. For convenience, we introduce the following notations:

Additional notations. For any iteration $t \in [T]$, model $g \in \mathcal{G}$, and stage $m \in [M]$, we define $K_{g,t}^m := \Phi_{g,t}^m (\Phi_{g,t}^m)^\top$, where $\Phi_{g,t}^m := [\phi(y_i)^\top]_{i \in \Psi_{g,t}^m}$. In addition, we denote by $0 < c_{g,t}^m \leq 1$ the lower bound in Lemma 6 corresponding to y_t and $K_{g,t}^m$. Let

$$\epsilon_{\text{RFF},g,t}^m \leq t^{-\frac{1}{2}} (|\Psi_{g,t}^m|)^{-1} \sqrt{G \cdot c_{g,t}^m}, \quad \Delta_{\text{RFF},g,t}^m \leq t^{-\frac{1}{2}} (|\Psi_{g,t}^m| (\|K_{g,t}^m\|_2 + \alpha))^{-1} \sqrt{G \cdot c_{g,t}^m} \quad (14)$$

denote the (upper bound of) error thresholds input to function COMPUTE_UCB_RFF.

$$\begin{aligned} & \sum_{g \in \mathcal{G}, m \in [M]} \sum_{t \in \Psi_{g,T+1}^m} \mathcal{B}_{g,t,1,t}^m \\ &= \sum_{g \in \mathcal{G}, m \in [M]} \sum_{t \in \Psi_{g,T+1}^m} (\alpha^{-1} |\Psi_{g,t}^m| \epsilon_{\text{RFF},g,t}^m + \alpha^{-2} \Delta_{\text{RFF},g,t}^m (\|K_{g,t}^m\|_2 + \alpha)) \\ &\leq \sqrt{G} \sum_{g \in \mathcal{G}, m \in [M]} \sum_{t \in \Psi_{g,T+1}^m} (\alpha^{-1} t^{-\frac{1}{2}} + \alpha^{-2} t^{-\frac{1}{2}}) \\ &\leq \sqrt{G} \sum_{t=1}^T (\alpha^{-1} t^{-\frac{1}{2}} + \alpha^{-2} t^{-\frac{1}{2}}) \\ &\leq O((\alpha^{-1} + \alpha^{-2}) \sqrt{GT}) \end{aligned} \quad (15)$$

where the first inequality holds by the fact that each $t \in [T]$ appears in at most one index set.

$$\begin{aligned} & \sum_{g \in \mathcal{G}, m \in [M]} \sum_{t \in \Psi_{g,T+1}^m} \mathcal{B}_{g,t,2,t}^m \\ &\leq \sum_{g \in \mathcal{G}, m \in [M]} \sum_{t \in \Psi_{g,T+1}^m} (c \cdot \alpha)^{-\frac{1}{2}} (2|\Psi_g| \alpha^{-2} \Delta_{\text{RFF},g,t}^m (\|K_{g,t}^m\|_2 + \alpha) + 3\alpha^{-1} |\Psi_{g,t}^m| \epsilon_{\text{RFF},g,t}^m) \\ &\leq \sqrt{G} \sum_{g \in \mathcal{G}, m \in [M]} \sum_{t \in \Psi_{g,T+1}^m} (2\alpha^{-\frac{5}{2}} t^{-\frac{1}{2}} + 3\alpha^{-\frac{3}{2}} t^{-\frac{1}{2}}) \\ &\leq \sqrt{G} \sum_{t=1}^T (2\alpha^{-\frac{5}{2}} t^{-\frac{1}{2}} + 3\alpha^{-\frac{3}{2}} t^{-\frac{1}{2}}) \\ &\leq O((\alpha^{-\frac{5}{2}} + \alpha^{-\frac{3}{2}}) \sqrt{GT}) \end{aligned} \quad (16)$$

Therefore, we conclude the proof. \square

B.3 Proof of Lemma 5

Proof. For convenience, we define $\tilde{k}_y := \tilde{\Phi}_g(\varphi(y)) \in \mathbb{R}^{|\Psi_g|}$, $Q := (K + \alpha I)^{-1} \in \mathbb{R}^{|\Psi_g| \times |\Psi_g|}$, and $\tilde{Q} := (\tilde{K} + \alpha I)^{-1} \in \mathbb{R}^{|\Psi_g| \times |\Psi_g|}$, where $\tilde{K} := \tilde{\Phi}_g \tilde{\Phi}_g^\top$. Using the same notations in the proof of

Lemma 1, we obtain that

$$\begin{aligned}
|\tilde{\mu}_g - \hat{\mu}_g| &= \left| (\varphi(y))^\top \tilde{\Phi}_g^\top (\tilde{K} + \alpha I)^{-1} v - k_y^\top (K + \alpha I)^{-1} v \right| \\
&= \left| \tilde{k}_y^\top \tilde{Q} v - k_y^\top Q v \right| \\
&\leq \left| \tilde{k}_y^\top (\tilde{Q} - Q) v \right| + \left| (\tilde{k}_y - k_y)^\top Q v \right|,
\end{aligned} \tag{17}$$

where we use Equation (22) to derive $\tilde{\mu}_g = (\varphi(y))^\top (\tilde{\Phi}_g^\top \tilde{\Phi}_g + \alpha I)^{-1} \tilde{\Phi}_g^\top v = (\varphi(y))^\top \tilde{\Phi}_g^\top (\tilde{K} + \alpha I)^{-1} v$ in the first equation.

1. Bounding $|\tilde{k}_y - k_y|^\top Q v|$. We evoke (Rahimi and Recht, 2007b, Claim 1), which is rewritten in Lemma 8 using our notations. For a desired threshold $\epsilon_{\text{RFF}} > 0$, set

$$s = \frac{4(d+2)}{\epsilon_{\text{RFF}}^2} \log \left(\frac{\sigma_p^2}{(\delta/2) \cdot \epsilon_{\text{RFF}}^2} \cdot 2^8 \right).$$

Then, with probability at least $1 - \frac{\delta}{2}$, it holds that $\sup_{y, y' \in \mathcal{Y}} |(\varphi(y))^\top \varphi(y') - k(y, y')| \leq \epsilon_{\text{RFF}}$, and hence $\|\tilde{k}_y - k_y\|_\infty \leq \epsilon_{\text{RFF}}$. Therefore, we obtain

$$|(\tilde{k}_y - k_y)^\top Q v| \leq \|\tilde{k}_y - k_y\|_2 \cdot \|Q\|_2 \cdot \|v\|_2 \leq \epsilon_{\text{RFF}} \sqrt{|\Psi_g|} \cdot \alpha^{-1} \cdot \sqrt{|\Psi_g|} = \alpha^{-1} |\Psi_g| \epsilon_{\text{RFF}}, \tag{18}$$

where the last inequality holds by $\|Q\|_2 = \lambda_{\min}^{-1}(K + \alpha I) \leq \alpha^{-1}$ and $\|v\|_\infty \leq 1$.

2. Bounding $|\tilde{k}_y^\top (\tilde{Q} - Q) v|$. Note that

$$\begin{aligned}
|\tilde{k}_y^\top (\tilde{Q} - Q) v| &\leq \|\tilde{k}_y\|_2 \cdot \|\tilde{Q} - Q\|_2 \cdot \|v\|_2 \\
&\leq \sqrt{2|\Psi_g|} \cdot \|\tilde{Q} - Q\|_2 \cdot \sqrt{|\Psi_g|}
\end{aligned}$$

where the first inequality holds by the fact that $(\varphi(y))^\top \varphi(y_i) = (2/s) \sum_{j=1}^s \cos(w_j^\top y + b_j) \cos(w_{i,j}^\top + b_{i,j}) \leq 2$. To bound $\|\tilde{Q} - Q\|_2$, we evoke (Avron et al., 2017, Theorem 7), which is rewritten in Lemma 9. For a desired threshold $\Delta_{\text{RFF}} \leq 1/2$, the following inequality holds with probability at least $1 - \frac{\delta}{2}$:

$$(1 - \Delta_{\text{RFF}})(K + \alpha I) \preceq \tilde{K} + \alpha I$$

for $s \geq \frac{8|\Psi_g|}{3\alpha} \Delta_{\text{RFF}}^{-2} \log(32s_\alpha(K)/\delta)$. By Sherman-Morrison-Woodbury formula, i.e., $A^{-1} - B^{-1} = A^{-1}(B - A)B^{-1}$ where A and B are invertible, we derive

$$\begin{aligned}
&\|(\tilde{K} + \alpha I)^{-1} - (K + \alpha I)^{-1}\|_2 \\
&\leq \|(\tilde{K} + \alpha I)^{-1}\|_2 \cdot \|(K + \alpha I) - (\tilde{K} + \alpha I)\|_2 \cdot \|(K + \alpha I)^{-1}\|_2 \\
&\leq \alpha^{-2} \Delta_{\text{RFF}} (\|K\|_2 + \alpha)
\end{aligned} \tag{19}$$

where the last inequality holds by the fact that $\|(\tilde{K} + \alpha I)^{-1}\|_2, \|(K + \alpha I)^{-1}\|_2 \leq \alpha^{-1}$ and $\|(K + \alpha I) - (\tilde{K} + \alpha I)\|_2 \leq \Delta_{\text{RFF}}(K + \alpha I)\|_2 \leq \Delta_{\text{RFF}}(\|K\|_2 + \alpha)$.

3. Putting everything together. Combining Equations (18) and (19), with probability at least $1 - \delta$, it holds that

$$|\tilde{\mu}_g - \hat{\mu}_g| \leq \alpha^{-1} |\Psi_g| \epsilon_{\text{RFF}} + \alpha^{-2} \Delta_{\text{RFF}}(\|K\|_2 + \alpha)$$

when

$$s \geq \max \left\{ \frac{4(d+2)}{\epsilon_{\text{RFF}}^2} \log \left(\frac{\sigma_p^2}{(\delta/2) \cdot \epsilon_{\text{RFF}}^2} \cdot 2^8 \right), \frac{8|\Psi_g|}{3\alpha} \Delta_{\text{RFF}}^{-2} \log \left(\frac{32s_\alpha(K)}{\delta} \right) \right\},$$

which concludes the proof. \square

B.4 Proof of Lemma 6

Proof. We use the same notations in the proof of Lemma 5. Let c denote a lower bound of $1 - \|k_y\|_{(K+\alpha I)^{-1}}^2$. Note that

$$\begin{aligned} & |\tilde{\sigma}_g - \hat{\sigma}_g| \\ &= \alpha^{-\frac{1}{2}} \left| \sqrt{1 - (\varphi(y))^\top \tilde{\Phi}_g^\top (\tilde{K} + \alpha I)^{-1} \tilde{\Phi}_g(\varphi(y))} - \sqrt{1 - k_y^\top (K + \alpha I)^{-1} k_y} \right| \\ &\leq (c \cdot \alpha)^{-\frac{1}{2}} \left| (\varphi(y))^\top \tilde{\Phi}_g^\top (\tilde{K} + \alpha I)^{-1} \tilde{\Phi}_g(\varphi(y)) - k_y^\top (K + \alpha I)^{-1} k_y \right| \\ &= (c \cdot \alpha)^{-\frac{1}{2}} \left| \tilde{k}_y^\top \tilde{Q} \tilde{k}_y - k_y^\top Q k_y \right| \\ &\leq (c \cdot \alpha)^{-\frac{1}{2}} \left(\left| \tilde{k}_y^\top (\tilde{Q} - Q) \tilde{k}_y \right| + \left| (\tilde{k}_y - k_y)^\top Q \tilde{k}_y \right| + \left| k_y^\top Q (\tilde{k}_y - k_y) \right| \right) \\ &\leq (c \cdot \alpha)^{-\frac{1}{2}} \left(\|\tilde{k}_y\|_2^2 \|\tilde{Q} - Q\|_2 + \|\tilde{k}_y - k_y\|_2 \|\tilde{k}_y\|_2 \|Q\|_2 + \|\tilde{k}_y - k_y\|_2 \|k_y\|_2 \|Q\|_2 \right) \\ &\leq (c \cdot \alpha)^{-\frac{1}{2}} \left(2|\Psi_g| \alpha^{-2} \Delta_{\text{RFF}}(\|K\|_2 + \alpha) + 3\alpha^{-1} |\Psi_g| \epsilon_{\text{RFF}} \right) \end{aligned} \tag{20}$$

which concludes the proof. \square

B.5 Analysis of Lemma 2

Proof. Solving KRR with n regression data requires $\Theta(n^3)$ time and $\Theta(n^2)$ space. Hence, by the convexity of the cubic and quadratic functions, the time for COMPUTE_UCB scales with $\Theta(\sum_{g \in \mathcal{G}} n_g^3) = O(t^3/G^2)$, and the space scales with $\Theta(\sum_{g \in \mathcal{G}} n_g^2) = O(t^2/G)$, where $n_g := |\Psi_g|$ is the visitation to any model $g \in \mathcal{G}$ up to iteration t , and we have $\sum_{g \in \mathcal{G}} n_g = t$. On the other hand, solving KRR with n regression data and random features of size s requires $O(ns^2)$ time and $O(ns)$ space. Therefore, the time for COMPUTE_UCB_RFF scales with $O(\sum_{g \in \mathcal{G}} n_g s^2) = O(ts^2)$, and the space scales with $O(\sum_{g \in \mathcal{G}} n_g s) = O(ts)$. \square

C Auxiliary Lemmas

C.1 Proof of Lemma 1

Proof. We rewrite the proof using the notations in Section 5. Obviously, Equation (5) holds when the index set Ψ_g is empty. In the following, we consider non-empty Ψ_g . Let $\Phi_g := [\phi(y_i)^\top]_{i \in \Psi_g}$.

Note that $k_y = [k(y, y_i)]_{i \in \Psi_g}^\top = \Phi_g(\phi(y))$ and $K = [k(y_i, y_j)]_{i, j \in \Psi_g} = \Phi_g \Phi_g^\top$. We have

$$\begin{aligned} \hat{\mu}_g - s_g(y) &= (\phi(y))^\top \Phi_g^\top (K + \alpha I)^{-1} v - (\phi(y))^\top w_g^* \\ &= (\phi(y))^\top (\Phi_g^\top \Phi_g + \alpha I)^{-1} \Phi_g^\top v - (\phi(y))^\top (\Phi_g^\top \Phi_g + \alpha I)^{-1} (\Phi_g^\top \Phi_g + \alpha I) w_g^* \\ &= (\phi(y))^\top (\Phi_g^\top \Phi_g + \alpha I)^{-1} \Phi_g^\top (v - \Phi_g w_g^*) - \alpha (\phi(y))^\top (\Phi_g^\top \Phi_g + \alpha I)^{-1} w_g^*, \end{aligned} \quad (21)$$

where the second equation holds by the positive definiteness of both matrices $(K + \alpha I)$ and $(\Phi_g^\top \Phi_g + \alpha I)$ and hence

$$\Phi_g^\top (K + \alpha I)^{-1} = (\Phi_g^\top \Phi_g + \alpha I)^{-1} \Phi_g^\top. \quad (22)$$

1. Bounding $(\phi(y))^\top (\Phi_g^\top \Phi_g + \alpha I)^{-1} \Phi_g^\top (v - \Phi_g w_g^*)$. Note that the scores $\{s_t : t \in \Psi_g\}$ are independent by the construction of Φ_g and $\mathbb{E}[s_t] = (w_g^*)^\top \phi(y_t)$, we have that

$$(\phi(y))^\top (\Phi_g^\top \Phi_g + \alpha I)^{-1} \Phi_g^\top (v - \Phi_g w_g^*) = \sum_{i=1}^{|\Psi_g|} [(\phi(y))^\top (\Phi_g^\top \Phi_g + \alpha I)^{-1} \Phi_g^\top]_i \cdot [v - \Phi_g w_g^*]_i$$

are the summation of zero mean independent random variables, where we denote by $[\cdot]_i$ the i -th element of a vector. Further, each variable satisfies that

$$\begin{aligned} & \left| [(\phi(y))^\top (\Phi_g^\top \Phi_g + \alpha I)^{-1} \Phi_g^\top]_i \cdot [v - \Phi_g w_g^*]_i \right| \\ & \leq \|(\phi(y))^\top (\Phi_g^\top \Phi_g + \alpha I)^{-1} \Phi_g^\top\| \cdot |[v - \Phi_g w_g^*]_i| \\ & \leq \sqrt{(\phi(y))^\top (\Phi_g^\top \Phi_g + \alpha I)^{-1} \Phi_g^\top \Phi_g (\Phi_g^\top \Phi_g + \alpha I)^{-1} (\phi(y))} \cdot (1 + \|w_g^*\|) \\ & \leq 2\hat{\sigma}_g \end{aligned}$$

where the last inequality holds by $\|w_g^*\| \leq 1$ and the second inequality holds by

$$\begin{aligned} \hat{\sigma}_g &= \alpha^{-\frac{1}{2}} \sqrt{k(y, y) - k_y^\top (K + \alpha I)^{-1} k_y} \\ &= \alpha^{-\frac{1}{2}} \sqrt{(\phi(y))^\top (\phi(y)) - (\phi(y))^\top \Phi_g^\top (K + \alpha I)^{-1} \Phi_g (\phi(y))} \\ &= \alpha^{-\frac{1}{2}} \sqrt{(\phi(y))^\top (I - (\Phi_g^\top \Phi_g + \alpha I)^{-1} \Phi_g^\top \Phi_g) (\phi(y))} \\ &= \sqrt{(\phi(y))^\top (\Phi_g^\top \Phi_g + \alpha I)^{-1} (\phi(y))}, \end{aligned}$$

Then, by Azuma-Hoeffding inequality, it holds that

$$\begin{aligned} & \mathbb{P} \left(|(\phi(y))^\top (\Phi_g^\top \Phi_g + \alpha I)^{-1} \Phi_g^\top (v - \Phi_g w_g^*)| > 2\eta \hat{\sigma}_g \right) \\ & \leq 2 \exp \left(-\frac{\hat{\sigma}_g^2 \eta^2}{2|\Psi_g| \hat{\sigma}_g^2} \right) \\ & \leq 2 \exp(-\eta^2/2) \end{aligned} \quad (23)$$

2. Bounding $\alpha(\phi(y))^\top(\Phi_g^\top\Phi_g + \alpha I)^{-1}w_g^*$. By the Cauchy-Schwarz inequality, it holds that

$$\begin{aligned}
& \left| (\phi(y))^\top(\Phi_g^\top\Phi_g + \alpha I)^{-1}w_g^* \right| \\
& \leq \|w_g^*\| \cdot \|(\phi(y))^\top(\Phi_g^\top\Phi_g + \alpha I)^{-1}\| \\
& = \|w_g^*\| \cdot \sqrt{(\phi(y))^\top(\Phi_g^\top\Phi_g + \alpha I)^{-1}\alpha^{-1}\alpha I(\Phi_g^\top\Phi_g + \alpha I)^{-1}(\phi(y))} \\
& \leq \alpha^{-1/2} \sqrt{(\phi(y))^\top(\Phi_g^\top\Phi_g + \alpha I)^{-1}(\Phi_g^\top\Phi_g + \alpha I)(\Phi_g^\top\Phi_g + \alpha I)^{-1}(\phi(y))} \\
& = \alpha^{-1/2} \hat{\sigma}_g,
\end{aligned} \tag{24}$$

where the second inequality holds by the positive definiteness of $\Phi_g^\top\Phi_g$.

3. Putting everything together. Plugging (23) and (24) in (21) and setting $\delta = 2\exp(-\eta^2/2)$ concludes the proof. \square

C.2 Proof of Lemma 4

Proof. The first statement holds by both Lemma 3 and Lemma 1, and a uniform bound over all $t \in [T], g \in \mathcal{G}$, and $m \in [M]$. Let $g_{\star,t} := \arg \max_{g \in \mathcal{G}} s_g(y_t)$ is the optimal model for prompt y_t and $\hat{g}_{\star,t}^m := \arg \max_{g \in \hat{\mathcal{G}}_t^m} \hat{s}_{g,t}^m$ is optimistic model at stage m .

To show the second statement, first note that $g_{\star,t} \in \hat{\mathcal{G}}_t^1$. Assume $g_{\star,t} \in \hat{\mathcal{G}}_t^m$ for some $m \in [M-1]$. Then, by the first statement, we obtain that $\hat{s}_{g_{\star,t},t}^m - \max_{g \in \hat{\mathcal{G}}_t^m} \hat{s}_{g,t}^m \geq s_{g_{\star,t}}(y_t) - (2\eta + \sqrt{\alpha}) \cdot \hat{\sigma}_{g_{\star,t}}^m - (s_{\hat{g}_{\star,t}^m}(y_t) + (2\eta + \sqrt{\alpha}) \cdot \hat{\sigma}_{\hat{g}_{\star,t}^m,t}^m) \geq -(2\eta + \sqrt{\alpha}) \cdot (\hat{\sigma}_{g_{\star,t}}^m + \hat{\sigma}_{\hat{g}_{\star,t}^m,t}^m) \geq 2 \cdot 2^{-m} = 2^{1-m}$, which ensures $g_{\star,t} \in \hat{\mathcal{G}}_t^{m+1}$.

Finally, by the first two statements, we have that $s_{\star}(y_t) - s_g(y_t) \leq \hat{s}_{g_{\star,t},t}^m + 2(2\eta + \sqrt{\alpha}) \cdot \hat{\sigma}_{g_{\star,t}}^m - (\hat{s}_{g,t}^m - 2(2\eta + \sqrt{\alpha}) \cdot \hat{\sigma}_{g,t}^{m,t}) \leq 2 \cdot 2^{1-m} = 2^{3-m}$. We conclude the proof. \square

C.3 Useful Lemmas

Lemma 8 (Rahimi and Recht (2007b), Claim 1). *Let \mathcal{M} be a compact subset of \mathbb{R}^d with diameter $\text{diam}(\mathcal{M})$. Then, for the mapping $\varphi : \mathbb{R}^d \rightarrow \mathbb{R}^s$ defined in Equation (3), we have*

$$\mathbb{P} \left(\sup_{y, y' \in \mathcal{M}} |(\varphi(y))^\top \varphi(y') - k(y, y')| \geq \epsilon \right) \leq 2^8 \left(\frac{\sigma_p \cdot \text{diam}(\mathcal{M})}{\epsilon} \right)^2 \exp \left(-\frac{s\epsilon^2}{4(d+2)} \right),$$

where $\sigma_p^2 := \mathbb{E}_p[\omega^\top \omega]$ is the second moment of the Fourier transform of k .⁶ Further, $\sup_{y, y' \in \mathcal{M}} |(\varphi(y))^\top \varphi(y') - k(y, y')| \leq \epsilon$ with any constant probability when $s = \Omega((d/\epsilon^2) \log(\sigma_p \cdot \text{diam}(\mathcal{M})/\epsilon))$.

Lemma 9 (Avron et al. (2017), Theorem 7). *Let $K = [k(y_i, y_j)]_{i,j \in [n]}$ denote the Gram matrix of $\{y_i \in \mathbb{R}^d\}_{i=1}^n$, where k is a shift-invariant kernel function. Let $\Delta \leq 1/2$ and $\delta \in (0, 1)$. Assume that $\|K\|_2 \geq \alpha$. If we use $s \geq \frac{8n}{3\alpha} \Delta^{-2} \log(16s_\alpha(K)/\delta)$ random Fourier features, then with probability at least $1 - \delta$, it holds that*

$$(1 - \Delta)(K + \alpha I) \preceq \tilde{K} + \alpha I \preceq (1 + \Delta)(K + \alpha I)$$

⁶For the RBF kernel with parameter σ^2 , i.e., $k_{\text{RBF}}(y, y') = \exp(-\frac{1}{2\sigma^2} \|y - y'\|_2^2)$, we have $\sigma_{\text{RBF}}^2 = \frac{d}{\sigma^2}$.

where $s_\alpha(K) := \text{Tr}[(K + \alpha I)^{-1}K]$ and we denote by $\tilde{K} = [(\varphi(y_i))^\top(\varphi(y_j))]_{i,j \in [n]}$ the approximated Gram matrix using $s \in \mathbb{N}_+$ random Fourier features, where $\varphi : \mathbb{R}^d \rightarrow \mathbb{R}^s$ is the feature mapping.

Lemma 10 (Valko et al. (2013), Lemma 4). *For any model $g \in \mathcal{G}$ and stage $m \in [M]$, let $\lambda_{g,1}^m \geq \lambda_{g,2}^m \geq \dots$ denote the eigenvalues (in the decreasing order) of the matrix $(\Phi_g^m)^\top \Phi_g^m + \alpha I$, where $\Phi_g^m = [\phi(y_i)^\top]_{i \in \Psi_{g,T+1}^m}$. Then, for any iteration $t \in [T]$, it holds that*

$$\sum_{t \in \Psi_{g,T+1}^m} \hat{\sigma}_{g,t}^m \leq \tilde{O} \left(\sqrt{d_{\text{eff}} \left(10 + \frac{15}{\alpha} \right) |\Psi_{g,T+1}^m|} \right)$$

where $d_{\text{eff}} := \max_{g \in \mathcal{G}, m \in [M]} \min\{j \in \mathbb{N}_+ : j\alpha \log T \geq \Lambda_{g,j}^m\}$ and $\Lambda_{g,j}^m := \sum_{i > j} \lambda_{g,i}^m - \alpha$ is the effective dimension.

D Additional Experimental Details and Results

1. Varying rankings of text-to-image models. We provide more examples showing that prompt-based generative models can outperform for text prompts from certain categories while underperforming for other text categories (see Figures 5, 6, and 8).

2. Prompt-based selection over three T2I models. See Figure 10.

3. Adaptation to new models and prompts. See Figures 11 and 12.

4. Implementation details. We use the CLIP-based features of the prompts as the context vector (Cherti et al., 2023) for tasks of T2I and T2V generation, and we use the CLIP-based features of the images in the task of image captioning. We set both the exploration and regularization parameters $\alpha, \eta = 1$ in all the experiments. Two hyperparameters have to be chosen. The first one is the parameter γ in the polynomial and radial basis function (RBF) kernels, which are given by

$$k_{\text{poly3}}^\gamma(x_1, x_2) = (\gamma \cdot x_1^\top x_2 + 1)^3, \quad k_{\text{RBF}}^\gamma(x_1, x_2) = \exp(-\gamma \cdot \|x_1 - x_2\|^2).$$

In the experiments, we select γ to be 5 and 1 for the polynomial and RBF kernel functions, respectively. The second hyperparameter is the number of random features in the RFF-UCB algorithm. In addition, the features are generated once for each sample and stored to save the computation of the RFF-UCB algorithm.

5. Ablation study on hyperparameters. We conduct ablation studies on the selections of parameter γ in the RBF kernel function and the number of features in RFF-UCB. The results are summarized in Figures 13 and 14, respectively. We select $\gamma = 1$ (default), 3, 5, and 7, and the number of features varying between 25, 50 (default), 75, and 100. Results show that the RFF-UCB algorithm can attain consistent performance. Additionally, we test the PAK-UCB-poly3 algorithm with $\gamma = 1, 3, 5$ (default), and 7 in the polynomial kernel and regularization parameter $\alpha = 0.5, 1.0$ (default), and 1.5 in KRR. The results are summarized in Figures 15 and 16, respectively.

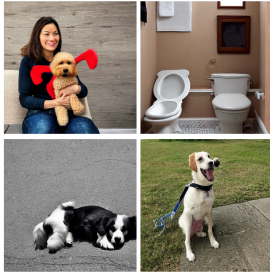



	Stable Diffusion v1.5	PixArt- α	Examples (clockwise)
Prompts of Type “dog”			<ol style="list-style-type: none"> 1. “a woman sitting with her dog and a toy” 2. “the little dog stands near the toilet in a small bathroom” 3. “a dog on a leash drinking water from a water bottle” 4. “a dog laying on the floor next to a door”
avg.CLIPScore	36.37 (± 0.13)	37.24 (± 0.09)	
Prompts of Type “car”			<ol style="list-style-type: none"> 1. “a motorcycle is on the road behind a car” 2. “two cars and a motorcycle on a road being crossed by a herd of elephants” 3. “a car that had run over a red fire hydrant” 4. “a taxi driving down a city street below tall white buildings”
avg.CLIPScore	36.10 (± 0.06)	35.68 (± 0.15)	

Figure 5: Prompt-based generated images from Stable Diffusion v1.5 and PixArt- α : Stable Diffusion v1.5 attains a higher CLIPScore in generating type-2 prompts (36.10 versus 35.68) while underperforms for type-1 prompts (36.37 versus 37.24).

6. Comparison of running time. We compare the running time of PAK-UCB and RFF-UCB, and the results are summarized in Figure 17.

7. Results on Other Conditional Generation Tasks

1. Text-to-Image (T2I). In this setup, we synthesize five T2I generators based on Stable Diffusion 2⁷, where each generator is an “expert” in generating images corresponding to a prompt type. The prompts are captions in the MS-COCO dataset from five categories: dog, car, carrot, cake, and bowl. At each iteration, a caption is drawn from a (random) category, and an image is generated from Stable Diffusion 2. If the learner does not select the expert generator, then we add Gaussian noise to the generated image. Examples are visualized in Figure 18.

2. Image Captioning. In this setup, the images are chosen from the MS-COCO dataset from five categories: dog, car, carrot, cake, and bowl. We synthesize five expert generators based on the vit-gpt2 model in the Transformers repository.⁸ If a non-expert generator is chosen, then the

⁷<https://huggingface.co/stabilityai/stable-diffusion-2>

⁸<https://huggingface.co/nlpconnect/vit-gpt2-image-captioning>





	UniDiffuser	PixArt- α	Examples (clockwise)
Prompts of Type “train”			<ol style="list-style-type: none"> 1. “the rusted out remains of a small railway line” 2. “a skier stands in the snow outside of a train 3. “train cars parked on a train track near a pile of construction material” 4. “several people on horses with a train car in the background”
avg.CLIPScore	35.29 (± 0.08)	34.25 (± 0.12)	
Prompts of Type “baseball bat”			<ol style="list-style-type: none"> 1. “a man in red shirt holding a baseball bat” 2. “a woman holding a baseball bat with her head resting on it” 3. “baseball player in the batter’s box hitting a baseball 4. “hind view of a baseball player, an umpire, and a catcher”
avg.CLIPScore	32.51 (± 0.05)	34.30 (± 0.04)	

Figure 6: Prompt-based generated images from UniDiffuser (Bao et al., 2023) and PixArt- α : UniDiffuser attains a higher CLIPScore in generating type “train” prompts (35.29 versus 34.25) while underperforms for type “baseball bat” prompts (32.51 versus 34.30).

caption is generated from the noisy image perturbed by Gaussian noises. Examples are visualized in Figure 20. The numerical results are summarized in Figure 21.

3. Text-to-Video (T2V). We provide numerical results on a synthetic T2V setting. Specifically, both the captions and videos are randomly selected from the following five categories of the MSR-VTT dataset (Xu et al., 2016): sports/action, movie/comedy, vehicles/autos, music, and food/drink. Each of the five synthetic arms corresponds to an expert in “generating” videos from a single category. Gaussian noises are applied to the video for non-experts. The results are summarized in Figure 22.

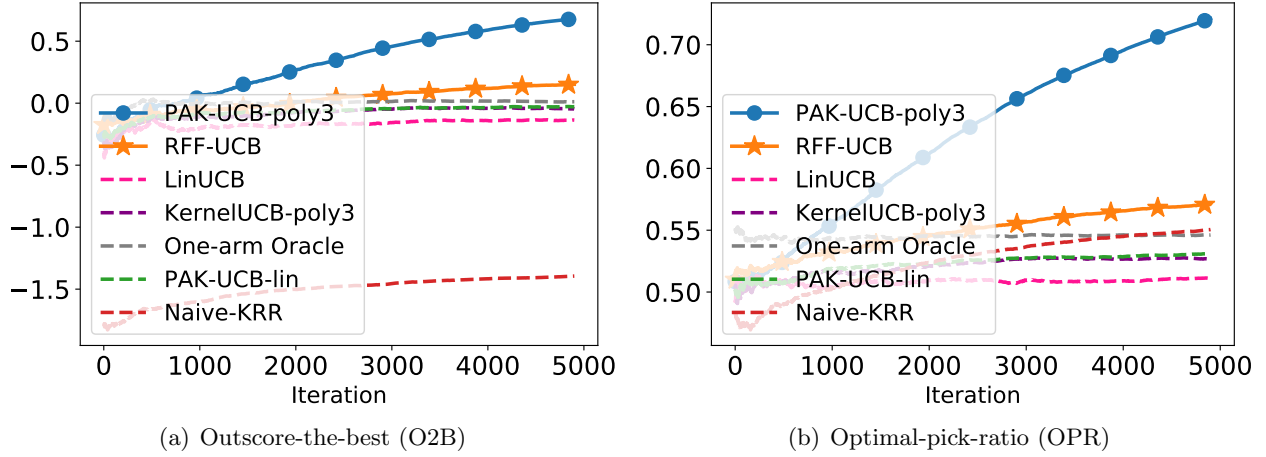


Figure 7: Prompt-based selection between UniDiffuser and PixArt- α (see Figure 6): Results are averaged over 20 trials.





	UniDiffuser	Stable Diffusion v1.5	Examples (clockwise)
Prompts of Type “elephant”			<ol style="list-style-type: none"> 1. “an elephant is carrying people across a forested area” 2. “an elephant has a sheet on its back 3. “a small gray elephant standing on a beach next to a lake” 4. “a large elephant in an open field approaching a vehicle”
avg.CLIPScore	36.67 (± 0.05)	35.08 (± 0.06)	
Prompts of Type “fire hydrant”			<ol style="list-style-type: none"> 1. “a fire hydrant in a clump of flowering bushes” 2. “a fire hydrant on a gravel ground with a fence behind it” 3. “a fire hydrant that is in the grass” 4. “a toy Ford truck next to a fire hydrant”
avg.CLIPScore	35.11 (± 0.14)	37.23 (± 0.05)	

Figure 8: Prompt-based generated images from UniDiffuser and Stable Diffusion v1.5: UniDiffuser attains a higher CLIPScore in generating type “elephant” prompts (36.67 versus 35.08) while underperforms for type “fire hydrant” prompts (35.11 versus 37.23).

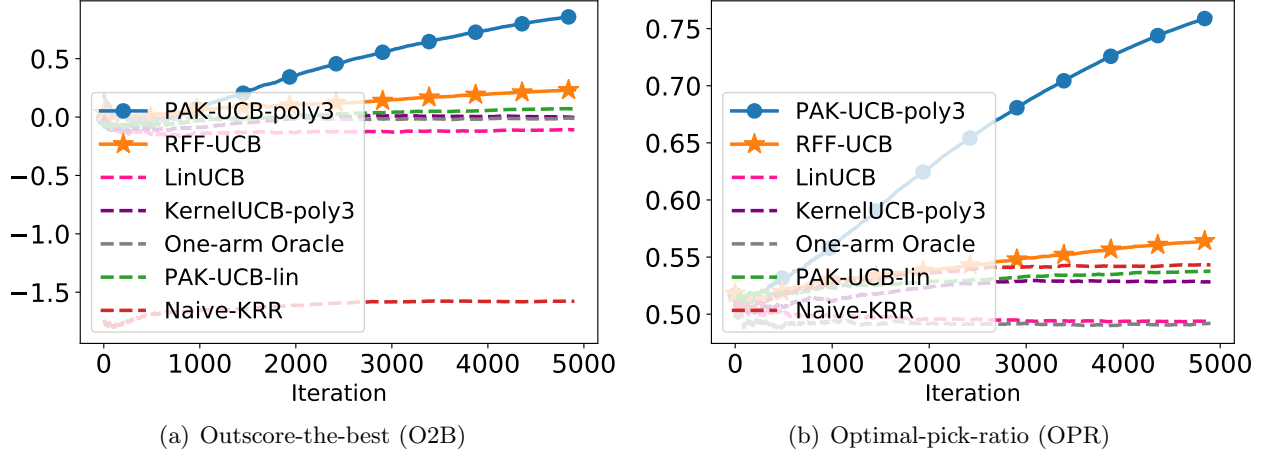


Figure 9: Prompt-based selection between UniDiffuser and Stable Diffusion v1.5 (see Figure 8): Results are averaged over 20 trials.

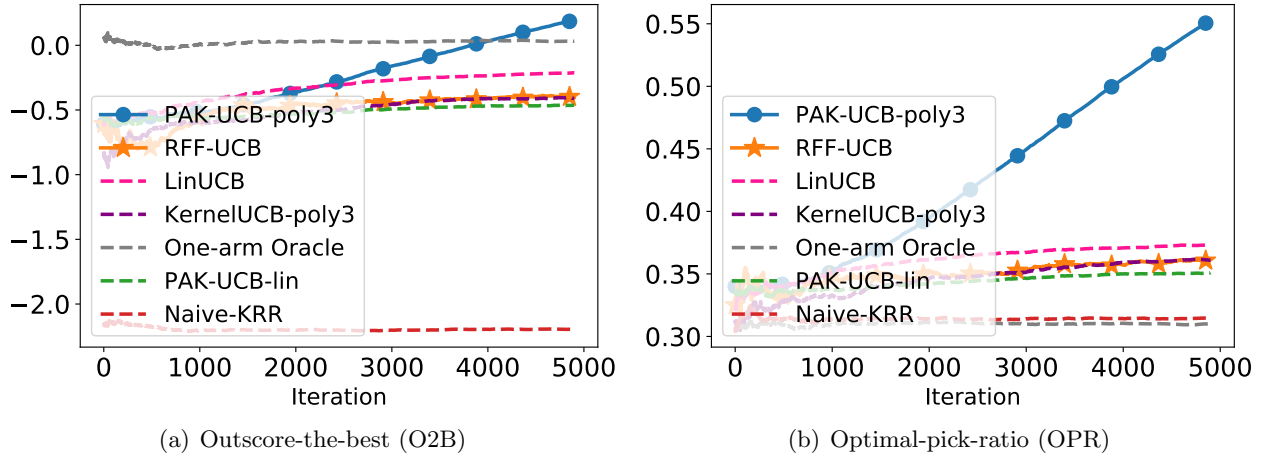


Figure 10: Prompt-based selection among Stable Diffusion v1.5, PixArt- α , and DeepFloyd: Prompts are drawn from types “carrot” and “bowl” in the MS-COCO dataset. Results are averaged over 20 trials.

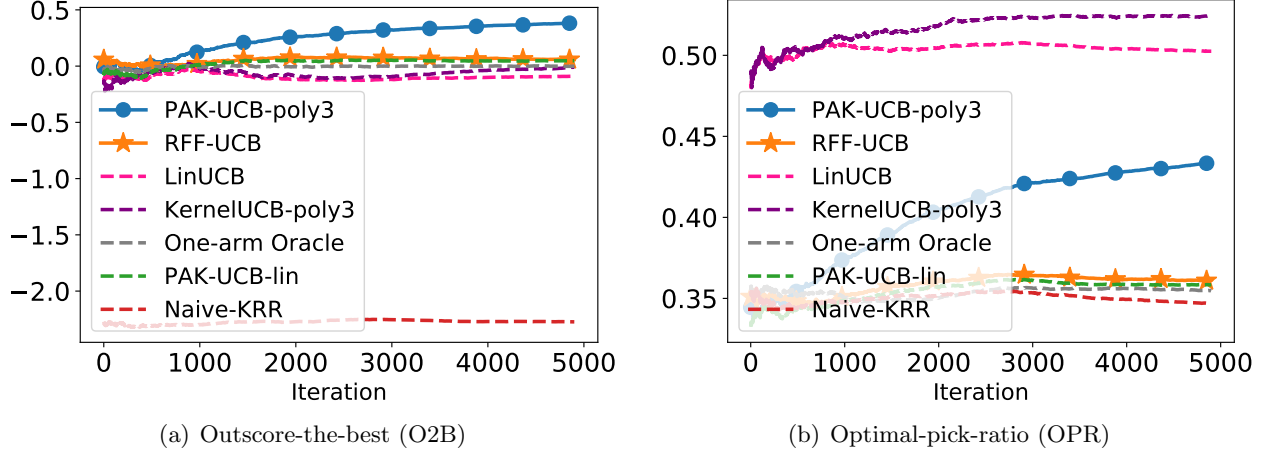


Figure 11: T2I generation with newly-introduced models: Initially, Stable Diffusion v1.5 and PixArt- α are available. UniDiffuser is introduced after 2500 iterations. Results are averaged over 20 trials.

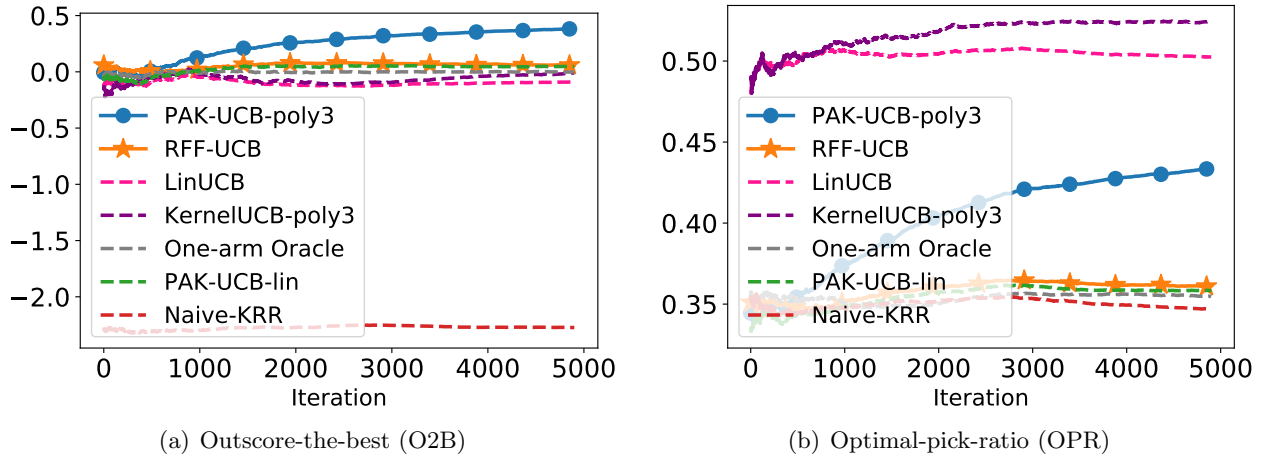
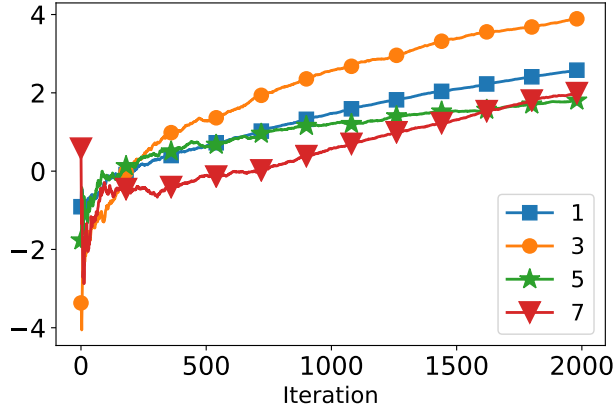
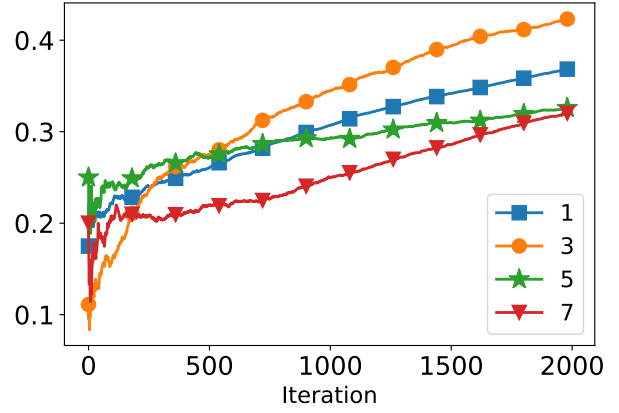


Figure 12: T2I generation with newly-introduced prompt types: Prompts are drawn from two categories in the MS-COCO dataset for the first 1k iterations. After that, an additional prompt category is added after each 1k iterations. Images are generated from PixArt- α and UniDiffuser. Results are averaged over 20 trials.

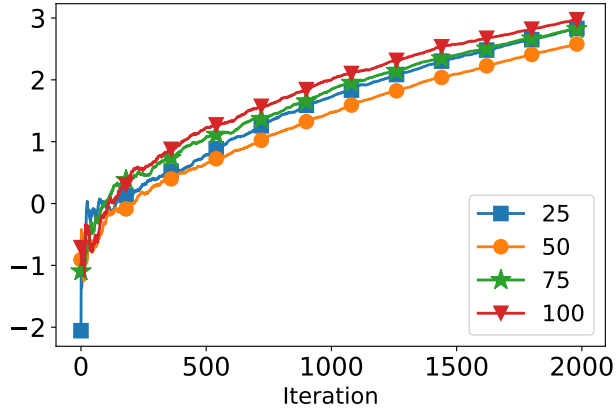


(a) Outscore-the-best (O2B)

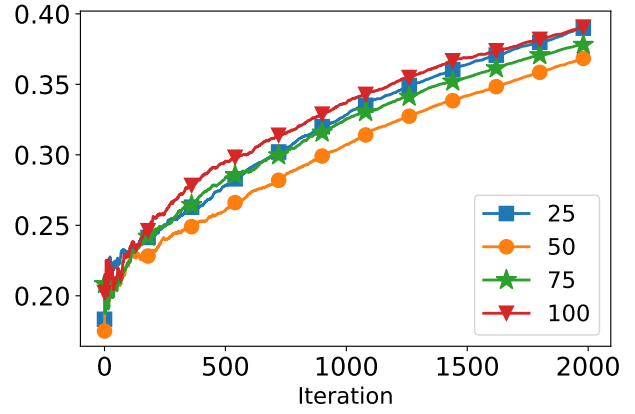


(b) Optimal-pick-ratio (OPR)

Figure 13: Parameter γ in the RBF kernel function: Results are averaged over 20 trials.



(a) Outscore-the-best (O2B)



(b) Optimal-pick-ratio (OPR)

Figure 14: Number of random features in RFF-UCB: Results are averaged over 20 trials.

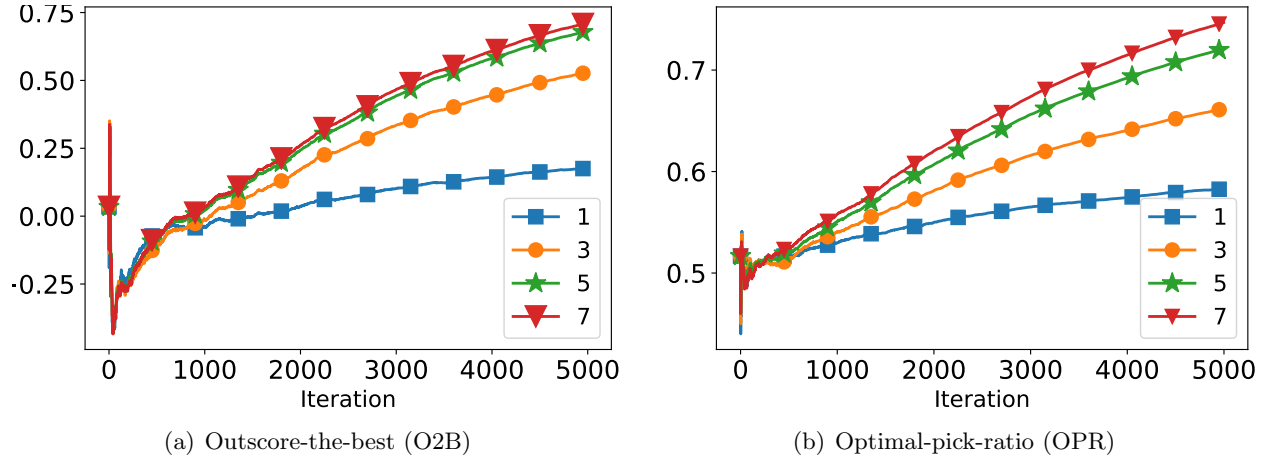


Figure 15: Parameter γ in the polynomial kernel function: Results are averaged over 20 trials.

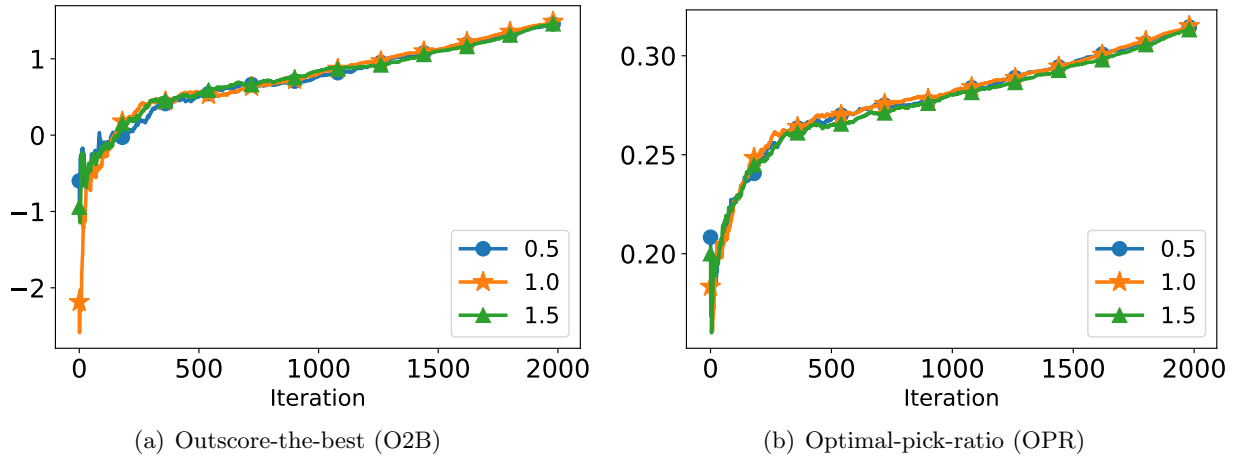


Figure 16: Regularization parameter α in KRR: Results are averaged over 20 trials.

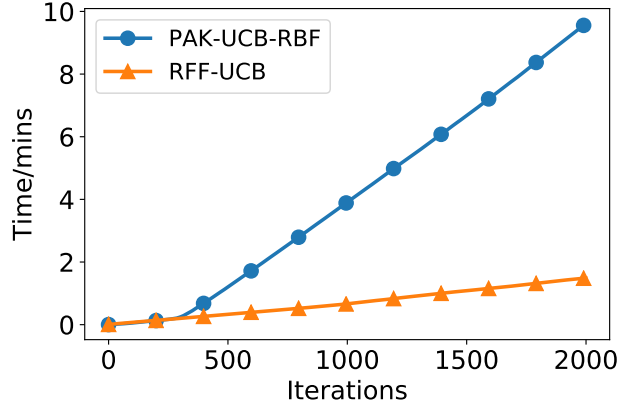


Figure 17: Running time: The execution time of PAK-UCB-RBF (PAK-UCB using the RBF kernel) and RFF-UCB on Setup 4. PAK-UCB-RBF takes around 10 minutes to finish 2,000 iterations of model selection, while RFF-UCB uses less than 2 minutes. Results are averaged over 20 trials.

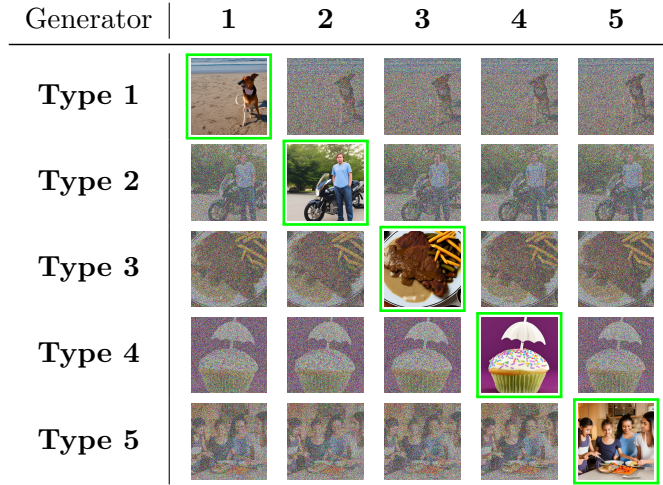


Figure 18: Generated images with noise perturbations: Each row and column display the generated images from a synthetic generator according to one single type of prompts. Images generated by the expert models are framed by green boxes. Gaussian noises are applied to non-expert models.

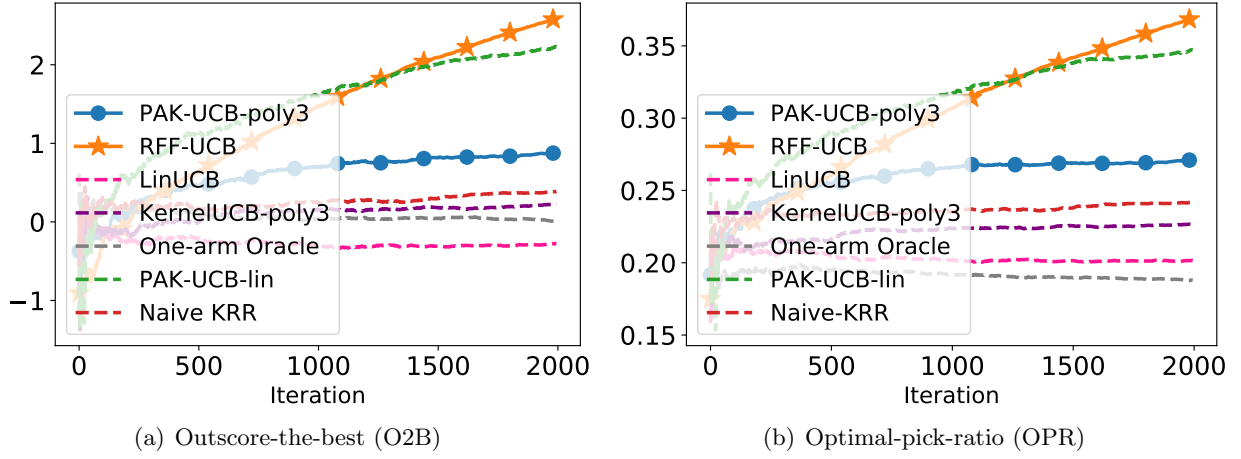


Figure 19: Synthetic expert model on text-to-image task: Results are averaged over 20 trials.







	Example 1	Example 2	Example 3
Clean	 <p><i>“a person on a surfboard in the air above the water”</i> 28.57</p>	 <p><i>“a man standing in a kitchen with a dog”</i> 40.53</p>	 <p><i>“a bowl filled with ice cream and strawberries”</i> 27.98</p>
Noisy	 <p><i>“a blurry photo of a skateboarder flying through the air”</i> 24.72</p>	 <p><i>“a cat that is standing in the grass”</i> 13.27</p>	 <p><i>“a blue and white bowl filled with water”</i> 25.83</p>

Figure 20: Generated captions for the clean and noise-perturbed images from vit-gpt2 and the corresponding CLIPScore.

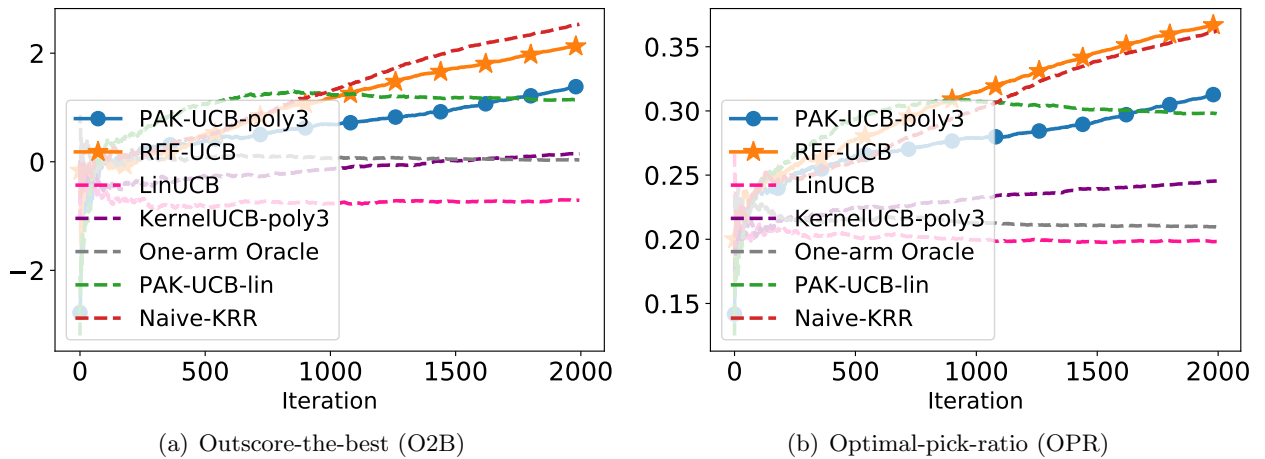


Figure 21: Synthetic expert model on image captioning task: Results are averaged over 20 trials.

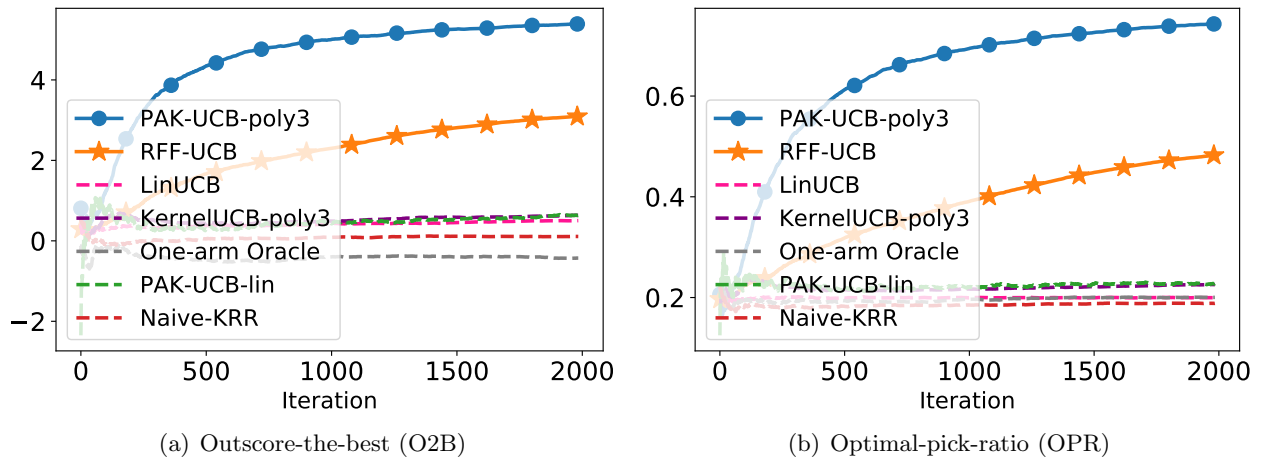


Figure 22: Synthetic expert model on text-to-video task: Results are averaged over 20 trials.